Comparison of a Finite-Difference and a Finite-Element Centered Finite-Volume Reservoir Simulator
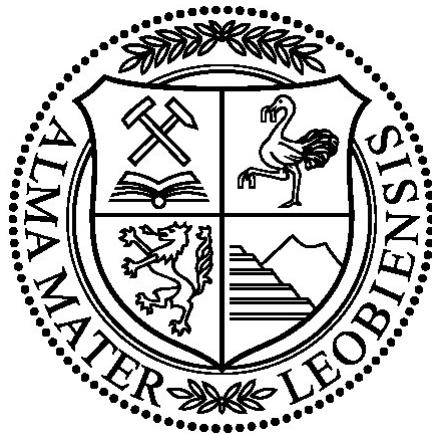
Ina Hadziavdic

Chair of Reservoir Engineering

Montan University of Leoben

Master Thesis

Leoben, 2015

Abstract

Classical reservoir simulation methods are based on first-order Finite Difference (FD) schemes applied to regular grids. Although widely used, these methods cannot resolve the sharp material interfaces and oblique faults in realistic models of reservoir geometries. When two-point flux approximations are used, finite difference solutions also exhibit strong grid orientation effects and fail to capture fingering instabilities. Using novel methods to overcome these drawbacks is inevitable. One new method that holds much potential is the Finite Element-Centered Finite Volume Method (FECFV).

In this study, water-flooding simulation results obtained with a commercial FD simulator for a complex faulted reservoir analog are compared with those from a FECFV prototype implemented on the basis of the Complex System Modeling Platform (CSMP++). The pseudo 2D cross-sectional model is based on a geological transect along the Chienberg tunnel in Switzerland. The same grid resolution was used for both simulators. The geological model was built in the SKUA- Paradigm and was exported to the commercial FD simulator. Rhinoceros was used to build the model and ICEM CFD to mesh it for the CSMP++ simulation.

The results reveal the influence of the different discretization schemes on the time to water breakthrough, cumulative oil production, flow velocity distributions, analytic versus discrete well model, and layer- and fault aspect ratios. The performance of the simulators in the presence of stark fault-country rock permeability contrasts have also been investigated.

Our study highlights the importance of an accurate treatment of material interfaces.

Kurzfassung

Klassische Reservoir Simulationsmethode basieren erstrangig auf Finite Difference (FD) Systemen, die bei regulären Gittern angewendet werden. Obwohl diese Methoden vielfach verwendet werden, können diese die scharfen Materialverbindungen und die Diagonalverwerfung nicht in realistischen Modellen der Lagerstättengeometrie klären. Wenn Zweipunkt Durchflussmengenannäherungen verwendet werden, zeigen die Finite Difference Solutions auch starke Gitterorientierungseffekte und scheitern daran, die Instabilität zu erfassen. Es ist unerlässlich, neuartige Methoden zu verwenden, um diese Nachteile zu überwinden. Eine neue Methode, die sehr viel Potential hat, ist die Finite Element-Centered Finite Volume Method (FECFV).

In dieser Studie werden Wasserflutungssimulationsergebnisse, die mit einem handelsüblichen FD Simulator für eine komplexe verworfene Lagerstättennachbildung erzielt wurden, mit jenen eines FECFV Prototyps verglichen, wobei dieser auf der Basis der Complex System Modeling Platform (CSMP++) implementiert wurde. Das Pseudo 2D Querschnittsmodell basiert auf einem geololgischen Profil des Chienbergtunnels in der Schweiz. Für beide Simulatoren wurde derselbe Gitterraster verwendet. Das geologische Modell wurde in SKUA- Paradigm gemacht und wurde anschließend an den handelsüblichen FD Simulator ausgegeben. Rhinoceros wurde verwendet, um das Modell zu bauen und ICEM CFD, um es für die CSMP++ Simulation zu vernetzen.

Die Ergebnisse zeigen den Einfluss der verschiedenen Diskretisierungssysteme zur Zeit des Wasserdurchbruchs, die kumulative Ölproduktion, Fließgeschwindigkeitsverteilungen, analytische im Vergleich zu eigenständigen Bohrloch Modellen, und in Hinsicht auf Schicht- und Verwerfungsverhältnisse. Die Leistung der Simulatoren bei einem starken Durchlässigkeitskontrast von Gebirgsgestein ist auch untersucht worden.

Unsere Studie zeigt die Bedeutung eines genauen Verfahrens der Materialverbindungen auf.

Declaration of authenticity

I declare in lieu of oath, that I wrote this thesis and performed the associated research myself, using only the literature cited in this thesis.

Ina Hadziavdic

June 2015

Acknowledgements

To my parents, whose love was the biggest support in the process of writing this thesis

Table of contents

List of tables

List of figures

Notation

B_o, oil formation volume factor

R_s, solution gas ratio

B_w, water formation volume factor

S_i, saturation of the phase i (w, wetting, n, nonwetting)

T_i, transmissibility of the phase i

ϕ, porosity

N, shape function

W, weight function

p_{ci}, capillary pressure of the phase i

f_w, fractional flow of water

q_i, flow velocity of the phase i

ρ_i, density of the phase i

Z, depth

g, gravitational acceleration

λ_i, fluid mobility of the phase i

F, flux

k, permeability

k_{ri}, relative permeability of the phase i

t, time

Superscripts:

n = old time level

n+1= new time level

x = old or new time level

Subscripts:

k = submatrix block index between 1 to J

m = matrix

o = oil

w = water

1. Introduction

This work aims to do a comparison between a simple cross-sectional model with flow from left to right by two different discretization methods and a complex model geologically built in SKUA (Paradigm product). Afterwards the complex model is simulated by CMG. The same geological model is built in Rhinoceros, meshed in ICEM CFD and exported to CSMP. Then various parameters such as recovery factor, oil cumulative production, analytic versus discrete well model, oil saturation, fluid pressure, flow velocity distributions, types of intersections and layer-fault aspect ratios, different fault permeability and grid resolution have been analyzed.

2. Theoretical Background

Because of the need to simulate reservoirs in a realistic way, reservoir simulation has been developed and widely used in the petroleum industry. The objective of reservoir study is primarily to predict performance of the reservoir and moreover to increase the ultimate recovery of the reservoir. Classical reservoir engineering is based on the gross average calculation, but it cannot predict heterogeneities and changes in parameters with space and time. Reservoir simulation is a special tool which is capable of capturing these changes. The reservoir is divided into smaller elements and flow equations are applied to each of them. The process of dividing the model into smaller elements is called discretization (Aziz and Settari, 1979).

2.1. Discretization Methods

In mathematics, discretization concerns the process of transferring continuous models and equations into discrete counterparts. This process is usually carried out as a first step toward making them suitable for numerical evaluation and implementation on digital computers. The most commonly used discretization methods are Finite Difference, Finite Volume and Finite Element methods.

Finite Difference discretization method

Finite Difference discretization method (FD) is the oldest method for numerical solution of Partial Differential Equations and believed to have been introduced by Euler in the 18th century. It is the easiest method for simple geometries. Transformations are needed to map a body-fitted grid into an orthogonal computational grid. Such transformation may not exist for a particular geometry or may be extremely cumbersome to perform.

The Finite Difference method utilizes a structured grid to perform calculations. It uses the differential form of the governing equations (mass, momentum and energy conservation laws) to formulate the mathematical discretization.

The coordinates of the different calculation points (depending on the dimension) are given by the following formulas:

$x_i = x_0 + i\Delta x$, with $i = 0,\ldots M_x$

$y_j = y_0 + i\Delta y$, with $j = 0,\ldots M_y$

$z_k = z_0 + i\Delta z$, with $k = 0,\ldots M_z$

Where Mx, My, and Mz are the number of points in each coordinate direction.

The coordinate vector is expressed as

$$x = \begin{bmatrix} x_0 \\ x_1 \\ . \\ . \\ x_{Mx} \end{bmatrix}, \quad x = \begin{bmatrix} x_0 & y_0 \\ x_1 & y_1 \\ . & . \\ . & . \\ x_{Mx} & y_{My} \end{bmatrix}, \quad x = \begin{bmatrix} x_0 & y_0 & z_0 \\ x_1 & y_1 & z_1 \\ . & . & . \\ . & . & . \\ x_{Mx} & y_{My} & z_{Mz} \end{bmatrix}$$

For 1D, 2D and 3D respectively.

Time can also be discretized:

$t^n = t^0 + n\Delta t$, with n=0,....

Three of the most common time discretization methods are:

1) FTCS: *Forward Time Centered Space method*

2) BTCS: *Backward Time Centered Space method*

3) CN: *Crank-Nicolson method*

After assembling the discrete problem, we get the matrix form: $Ap^{n+1} = Bp^n + F$

Finite Volume discretization method

Finite Volume discretization method (FVM) uses the integral form of the governing equations to formulate the mathematical discretization, as compared to FDM, which uses the differential form. It is also suitable for complex geometries, because it can be applied with any type of grid (structured or unstructured). Transformation of governing equations is not required. Alternatively, one may apply FVM in a transformed plane. It is mostly used for advection problems.

The mathematical basis for all integral form discretization methods lies in the ability to find functions W(**x**), also known as weight functions or trial functions. We can use these W(**x**) functions to aid us in the discretization process since we can choose them to be whatever we would like them to be.

Typically, information is cell-centered or node-centered, and accounting for movement of fluid from one finite volume cell to another is carried out through the calculation of "fluxes" at the cell "faces". We then "assemble" our governing equations by adding the contributions from all the cells involved by using the additive property of integrals.

Finite Element discretization method

Finite Element discretization method (FE) also uses the integral form of PDE's to generate formulations. This method does not guarantee mass conservation and it is mostly used for diffusion problems.

It is possible to derive and apply the finite element method in two ways. One way is through variational formulations and another one is through residual formulations.

Variational formulations are based on seeking the solution to the problem through the minimization of a *function* that expresses the total energy in the system. A clear example is the famous principle of least action*.*

The most common used method is **Method of Weighted Residuals**, as the starting point for a number of spatial discretization. It is based on the integral form of the governing equations and is the basis for assembling the finite element method solution, which will yield a matrix system of the form **Ka=f.** The mostly used solution method is Galerkin method. We get the solution assuming that the shape function (N_i) is equal to the weight function (W_i) (Aziz and Settari, 1979). In the contrast to FD approach, FE approach divides the domain into simply shaped regions, or elements (Chapra and Canale, 2010.)

Finite-Element Centered Finite Volume discretization method

Finite Element Centered Finite Volume (FECFV) method (Bazr-Afkan, 2012), is mainly developed for simulation of DFM models, spatially discretized by unstructured meshes in CSMP++ reservoir simulator package. The method accounts for viscous, capillary and gravitational forces and their interplay. The FECFV method acknowledges the effects of material discontinuities on the fluid flow which is very important for application to cross-sectional models of NFRs with large differences in material properties from the rock matrix to the fractures. Compared to the Control Volume Finite Element method, which is conservative on node centered control volumes, the FECFV method produces inter-element fluxes supporting volume or mass conservation on an elemental basis. Lower dimensional elements can be used as well, because transport is calculated on the element. For example, if we need to represent fractures, they become separate control volumes in the transport scheme and this makes flow in the fractures more independent of mesh resolution. This means that we can mesh the models with a lower number of elements. Transmissibility calculation is not needed, and this gives the advantage that elongated elements can be used in the mesh, in contrast to CVFE, where we need Delaunay triangulation mesh to avoid negative transmissibility. Computational time is saved by the method that keeps track of

elements which go through property changes and only includes them in the calculations when needed (Bazr-Afkan, 2012).

CMG simulator, a simulator which uses Finite Difference approach, in this thesis is compared to CSMP simulator, which uses FECFV approach.

2.2. Evaluation methods

To evaluate the results of the reservoir simulation, static and dynamic evaluation are tightly connected and their interplay in the reservoir simulation is of the great significance. Static means stationary or fixed, while dynamic means energetic and capable of action. Static features do not change over time. On the opposite, dynamic do.

2.2.1. Static evaluation

The most important properties of the static model are pore volume, initial oil in place, and boundary conditions. Static model starts with structure and grid modelling follows by facies and petrophysical modelling and at the end, simulations and upscaling are done. This is the 'boundary' between static and dynamic data, however there is no exact 'boundary' between these modeling workflows, because they interact with each other. Both of them are important and inevitable parts of the reservoir modeling workflow. Figure 1 shows the 3D Reservoir Modeling Workflow, which accompanies static and dynamic modeling.
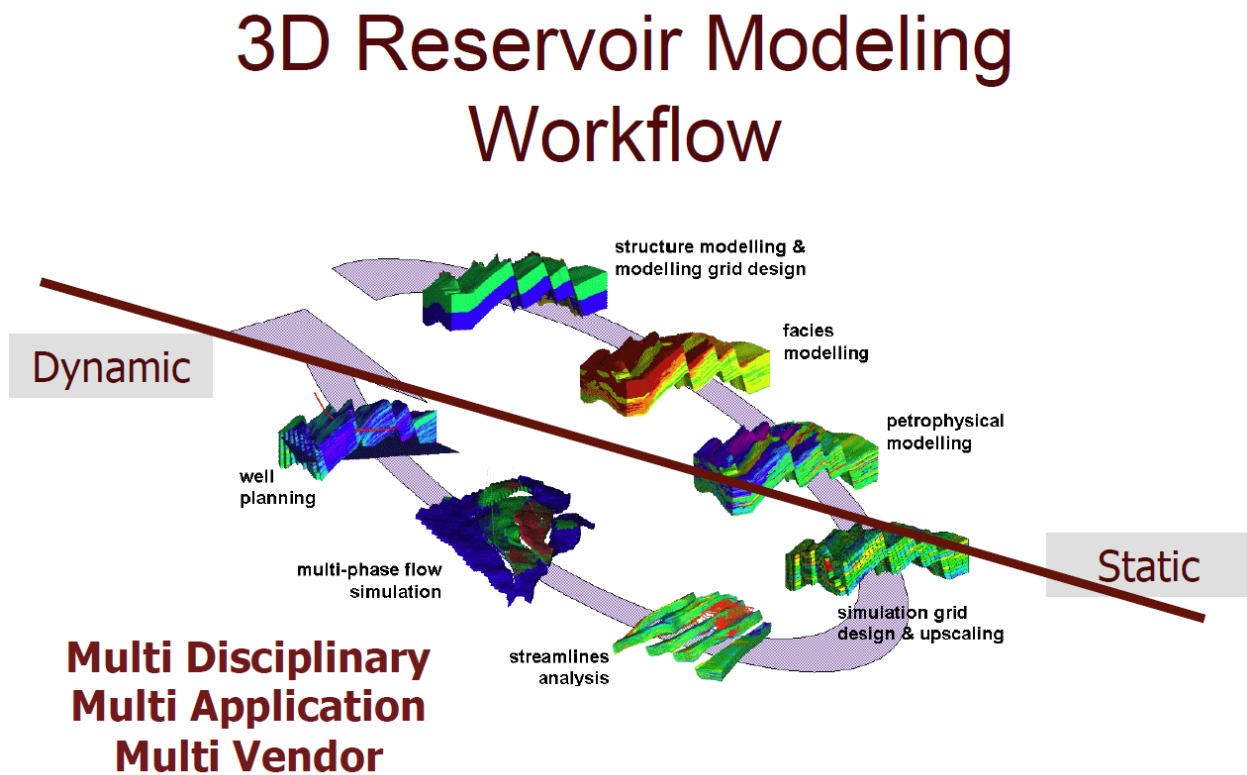
Figure 1: 3D Reservoir Modeling Workflow (King, 2011)

Pore volumes and initial oil in place

The prediction of hydrocarbon pore volumes and initial oil in place with uncertainties gives assistance to decisions in development of the particular reservoir fields (Berteig, 1988) .

There are a variety of methods which can be used for the pore volumes estimation. One of them is the Pore-Volume Method (Strausser, 1976). Most of the methods applied statistical approach, but a small number of them have found a suitable stochastic solution of the problem. The most important ones are the Monte Carlo simulations for estimation of oil in place and pore volumes (Delfiner, 1977;Behrenbruch, 1985). The Monte Carlo simulation is a conditional simulation, a geostatistical method for generation 2 or 3-dimensional fields of a given variable that are consistent with the observed data and have the same autocorrelation structure as a true field. This method is applied to the reservoir description parameters and the expectation curves of volumes in place are derived (Delfiner, 1977). Oil in place is the term which refers to the amount of total oil present in the reservoir. Oil in place can be calculated by following equation,

$$OIIP = 7.758 Ah\Phi(1 - S_w)/B_c$$

where A is area of interest, h is net pay, Φ is porosity, Sw water saturation and Bo is the oil formation volume factor (Murtha, 1997).

Estimation techniques of the reserves

Volumetric technique

The volumetric technique calculates the OIIP by taking into account the size of the reservoir as well as the physical properties of the fluids and rocks. The recovery factor is assumed and multiplied by the OIIP to get the reserves. This method is useful during the early life of the reservoir.

Material balance method

The material balance method utilizes the equation which relates volume of oil, water and gas that have been produced and, additionally, changes in reservoir pressure. This method needs to be done after some production from the reservoir has occurre

Production decline curve method

This method uses production data in order to fit a decline curve and estimate future oil production. The most common forms of decline curves are exponential, hyperbolic, and harmonic. The curve can be expressed mathematically or plotted on a graph to estimate future production. It has the advantage of (implicitly) including all reservoir characteristics.

Boundary conditions and simulation setup

Boundary conditions are very important in reservoir simulation in order to establish interplay between the reservoir and its surroundings. The most used boundary conditions are:

a) The Dirichlet boundary condition:

In the reservoir, the Dirichlet Boundary Condition happens when we apply fixed value like pressure or saturation at one of the boundaries or at the well.

b) The Neumann boundary condition: this boundary condition is used if we want to prescribe production rate, flow rate across the boundary, influx from the aquifer or flow from parts of the reservoir outside of the simulated domain. Flow across boundaries can be expressed with the source term as well (q).
c) The combination of the Dirichlet and Neumann boundary conditions:

mixed and Robin boundary conditions. The difference is that Robin boundary condition is a weighted combination of the Dirichlet and Neumann boundary conditions and mixed boundary conditions are specified on the different subsets of the boundary (Aziz and Settari, 1979).

Initial Conditions

The initial conditions for CSMP++ simulations (2-phase, incompressible flow) are entry pressure, S_w - initial saturation of water and S_o - initial saturation of oil.

The initial conditions for CMG simulations (for the reservoir initially containing water and oil-2 phase flow) are: reference pressure and depth, oil-water contact (OWC) and constant bubble point pressure.

2.2.2. Dynamic evaluation

The dynamic process starts with a severe analysis of the stratigraphic time record of the sedimentary column and the attribution of the absolute ages. In this way, an absolute time sequence of critical geological events is created and a conceptual geological process model is formed- the backbone of the dynamic process interpretation and the chain of logics for a computer model.

The goal of the petroleum simulation is to reconstruct the geological history of the petroleum system, from the origin to the present. The main focus of the reconstructing is the location and 3D configuration of the drainage areas for mature source rocks through time and possible migration pathways. The modeling of the petroleum system follows exact geological time. The main concepts and methods of this kind of modeling are well established in existing basin modeling techniques. It begins with the deposition and compaction of the oldest stratigraphic units at the bottom of the system and works its way upward through earlier and earlier events to the present day.

The resulting dynamic modeling requirements mean that our models must be able to take into account the most important changing factors through geologic time. These consist of:
- Hydrocarbon phase relationship changes as a function of temperature and pressure
- Change of the geometries.
-Overpressures which are caused by compaction disequilibrium and hydrocarbon generation.
- Non-steady-state, multi-dimensional thermal histories.

The most important dynamic properties are recovery factor, time to breakthrough, grid resolution, flow velocities distribution and cumulative oil production (Welte, 2002).

Recovery factor

One of the main goals of the majority of the companies is the increase of the recovery factor because it is becoming more difficult to discover new oil fields. The recovery factor is showing how much oil or gas can be produced from particular reservoir. Water flooding is currently being the most preferred technique among the others recovery techniques like polymer flooding, miscible gas injection, foam injection, CO_2 injection etc.

The factors affecting the recovery factor from water and gas flooding can be described by the following equation,

$$RF = E_{ps} \cdot E_s \cdot E_D \cdot E_C$$

RF is recovery factor defined as the volume of oil recovered over the volume of oil initially in place (OIIP), E_{ps} is microscopic displacement efficiency, E_s is macroscopic displacement efficiency, E_d is connected volume factor- the proportion of the total reservoir volume connected to the wells, E_c is economic efficiency factor (Muggeridge, 2013).

Time to breakthrough

Time to breakthrough is the time at which water starts to be produced from the reservoir. The goal is to prolong, as long as possible, this time in the production life of the reservoir and to maintain the wellhead pressure. Sometimes this is very hard to obtain due to the structure of the reservoir, position of the wells (if they are close to OWC), coning and injection and production rates. We prefer that the front of the injected fluid goes very smoothly and sweeps the whole volume between the two wells. However, this is not always possible due to the heterogeneities and reservoir fluid interactions which causes fingering. The problem related to the production of the water is usually a disposal problem which raises the costs of production. In order to prevent this problem, it is required to find suitable injection and production rates for the reservoir. If these rates are very high, it is possible to have very early breakthrough, but on the other hand, if these are too low, the cumulative oil production will be too low. So it is very important to optimize and find suitable rates.

Grid resolution to express instabilities

In order to represent the reservoir in a real way, complexities like the static features-structure and geology, and the dynamic features such as flow velocity distributions need to be included in the model. Very often, a reservoir contains faults or fractures, which need more refined mesh in order to simulate difficulties related to production near these structures. In this case, mesh refinement has a great role. Nowadays, there are more advanced methods of refinement, such as recursive coarsening. The goal of the refinement is to find an optimally coarsened grid. In the case that coarsening is carried too far, the reservoir description can be too homogenized, and in the case that coarsening is too little, the reservoir model costs can be very high. The method of recursive coarsening is using a sequential recursive coarsening algorithm. This algorithm proved to be faster than sequential refinement (King, 2006). Standard reservoir simulators do not show detailed interaction between the local pressure gradient, reservoir heterogeneity and well completion components. This is due to the effects which occur on very small scales compared to the typical simulation grid-blocks (Karimi-Fard, 2012).

The general approach for improving near-well representation is called Local Grid Refinement (LGR) (Heinemann, 1991). The model can capture flow behavior in detail by providing sufficient resolution in the near-well region. This approach is widely used because of its simplicity, but there are some problems related to it- like a large number of small cells in the near-well region which can have an effect on numerical stability and time-step.

The expanded well model concept is a new concept that was presented by Karimi-Fard and Durlofsky (2012). This approach has some similarities with the flow-based grid generation

techniques, but the difference is that it constructs flow-based grids only in the near-well region., not globally. The expanded well model includes near-well regions plus relevant regions of the reservoir. This model can capture fine-scale effects using fewer cells than LGR (Karimi-Fard, 2012).

Types of intersections of structures/layers

When modeling the reservoir, one usually needs, in order to represent the reservoir in a realistic way, to model different and complex intersections of the layers or structures. This also happens in this model. The influence of these intersections can be great, so one needs to carefully investigate the possible influences and results, to which this can lead.

As already said previously, because it was not possible to build such a complex model in CMG simulator, the model has been built in the SKUA Paradigm and output to CMG.

Building such a complex model was very challenging, due to the great number of faults, which are intersecting the layers at different angles and the small layers which are moved up or down depending on the nature of the faults- if the fault is normal or a reverse fault.

However, this was possible and less challenging to build in the Rhinoceros, and to then mesh in ICEM CFD. The resulting grid is an unstructured grid, at the opposite of the CMG grid, which is structured.

Permeability contrasts

Permeability is one of the key factors in determining the possibility to recover oil. This is the reason why it is so important, and why it is so often investigated. The reservoir that I observed is a reservoir with considerable permeability contrasts, which needs to be taken into account in the simulations. Permeability contrasts can cause different simulation problems, but beyond that, if the prediction is not very reliable, than it is possible to have problems during exploration and drilling as well.

Fault permeability- impermeable, low, high

Fault permeability is one of the properties which has a great influence on the flow in this model. As previously shown, there are 19 faults and as default, all faults are very permeable, what makes the flow easier. Faults can act as a conduit for a fluid flow or as a flow barrier. In the case of the flow barriers, the faults introduce compartmentalization that severely affects recovery and fluid distribution in the reservoir. In order to make reservoir simulation reliable, it is crucial to understand and incorporate the impact which faults have on fluid flow.

In order to represent the nature of the fault (sealing or non-sealing), CMG uses transmissibility multipliers, which are taking into account reduced or increased permeability for each cross-fault connection.

Transmissibility multipliers are strongly grid dependent and refer to the connection between two grid cells, rather than to the fault itself. The multiplier of 0 is used for sealing faults and 1 for non-sealing faults.

CSMP simulator adjusts the permeability of the faults directly in the configuration file. In this way, permeability are strongly dependent on the fault itself.

In the chapter Fault permeability (Results), different type of the fault permeability are simulated and compared to the initial model, which is originally the reservoir with highly permeable faults.

3. Governing equations

Governing equations are mathematical statements of the three fundamental physical laws: mass conservation, conservation of energy and momentum equation. Governing equations in both simulators, CSMP and CMG are the same, but in the following chapters is discussed in detail how these equations are derived.

3.1. CSMP++ governing equations

It is assumed that flow can be treated as a two phase immiscible flow of incompressible fluids. There is no mass transfer between phases and mass is conserved separately for each phase. Using the mass conservation law, combined with Darcy's law and auxiliary equations, which relate phase pressure and phase saturations, leads to this system of equations:

$$\frac{\partial}{\partial t}(\Phi S_w) = \nabla \cdot (k\lambda_w (\nabla p_w - \rho_w g \nabla z)\ ) + q_w$$

$$(3.1)$$

$$\frac{\partial}{\partial t}(\Phi S_w) = \nabla \cdot (k\lambda_n (\nabla p_n - \rho_n g \nabla z)) + q_n \tag{3.2}$$

$$p_c(S_w) = p_n - p_w \tag{3.3}$$

$$S_w + S_n = 1 \tag{3.4}$$

Since it is assumed that the fluid is incompressible, mass balance results to volume balance. Equations (3.1) and (3.2) are the volume balance equations for the wetting (w) and non-wetting (n) phase, respectively. Variable **k** is the absolute permeability tensor and Φ is porosity of the medium. Variables $p_\alpha, S_\alpha, \rho_\alpha$ and q_α are pressure, saturation, density and volume flow rate per volume of reservoir rock of phase α, where $\alpha = \{n, w\}$. The variable g is acceleration of gravity, and p_c is the capillary pressure function. The mobility of the phase α is given by the equation

$$\lambda_\alpha = \frac{k_{r\alpha}}{\mu_\alpha} \tag{3.5}$$

The equation system (3.1)-(3.4) can be solved in different ways (Aziz and Settari, 1979; Chen et al., 2006). The formulation with p_n and S_w as the principal solution variables is widely used in reservoir simulation. Equations can be decoupled, by expressing wetting phase pressure in terms of the non-wetting phase pressure and capillary pressure. Three main varieties of this approach are the phase formulation, the weighted formulation and the global pressure formulation. These formulations are the basis for a solution strategy called the Sequential Solution Method where governing pressure and transport equations are discretized separately and solved sequentially. This strategy is also used in IMPES method by Stone and Garder (1961). This simulator uses IMPES approach.

Coupling between pressure and saturation equations is reduced by defining global pressure (Chavent and Jaffre, 1986).

$$p = p_n - \int_{S_w} (f_w \frac{dp_c}{dS_w})(\xi)d\xi \tag{3.6}$$

Where f_w is water fractional flow function defines as,

$$f_w = \frac{\lambda_w}{\lambda_w + \lambda_n} \tag{3.7}$$

Using the pressure from (3.6) the total velocity equation is given now by

$$u_t = -k(\lambda_w + \lambda_n)\nabla p - (\lambda_w \rho_w + \lambda_n \rho_n)g\nabla z) \tag{3.8}$$

The following equation is derived from the sum of the equations (3.1) and (3.2),

$$-\nabla \cdot (k(\lambda_w + \lambda_n)\nabla p - (\lambda_w \rho_w + \lambda_n \rho_n)g\nabla z) = q_n + q_w \tag{3.9}$$

Neglecting the compressibility of the porous medium, saturation changes are then expressed by a saturation transport equation derived from equation (3.1.) for the wetting phase,

$$\Phi \frac{\partial S_w}{\partial t} = -\nabla \cdot (k f_w \lambda_n (\nabla p_c + (\rho_n - \rho_w)g\nabla z) + f_w u_t) + q_w \tag{3.10}$$

The equation (3.9) can be solved with finite element method and linear basis function, N_i.

An approximate solution $\hat{p}$ is found,

$$\hat{p}(x,y) = \sum_{i=1}^{m} N_i(x,y)p_i \tag{3.11}$$

Where p_i are the unknown pressure values at the nodes, and m is the number of nodes in the discretized domain. Then the weighted residual formulation is

$$\int_\Omega w(x,y)\; \nabla \cdot (k(\; \lambda_w + \lambda_n)\nabla \hat{p}(x,y) + (\lambda_w\rho_w + \lambda_n\rho_n)g\nabla z) + q_w + q_n)d\; V = 0 \qquad (3.12)$$

Where w(x,y) is a weighting function and Ω is the problem domain. By subdivision of the domain Ω into non-overlapping elements Ω_e, this integral can be expressed as a sum of integrals over each element. After the weakening of the strong form (3.12) and utilizing Galerkin method, we obtain,

$$\left[\sum_e \int_\Omega \nabla N^T k(\lambda_w + \lambda_n)\nabla N dV\right]p$$
$$= -\sum_e \int_\Omega \nabla N^T (\lambda_w\rho_w + \lambda_n\rho_n)g\nabla z dV + \sum_e \int_\Omega \nabla N^T (q_w + q_n)dV \qquad (3.13)$$

A summation sign is an assembled sum over the all elements in the domain, including the grid connectivity information. Beside discretizing properties on the nodes, they can be discretized also as piecewise constant values on the elements. In this approach, saturation and other fluid properties can be discontinuous from element to element. This has the many advantages, for example:

- material interfaces conform to the element faces
- using linear basis function produces velocities that are constant over the elements and it is enough just to calculate velocity in one point inside the element, most likely in the barycenter
- no need for transmissibility at the Node Centered Finite Volumes (NCFV) facets-each of them is constructed from as many sectors as there are parent elements sharing its central node(Figure 2)
- upstream and downstream mobility of NCFV are the same, because saturation is, piecewise constant over elements
- elements with high aspect ratios can be used without causing problems in the scheme (Bazr-Afkan, 2012).
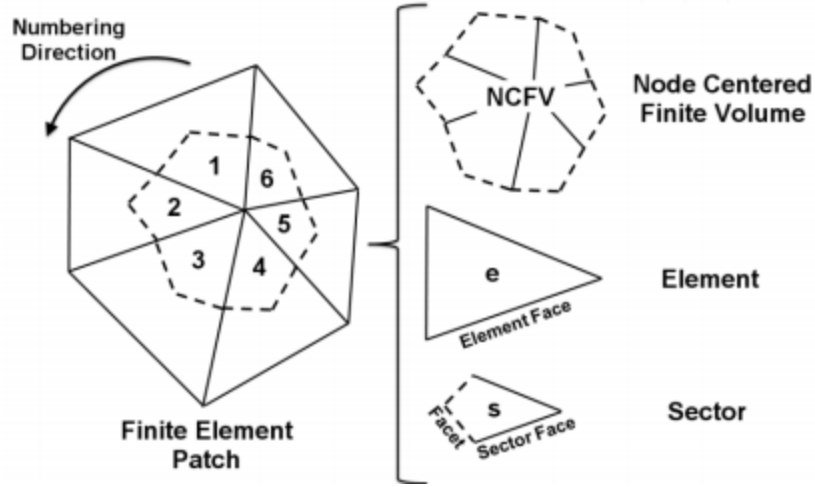
Figure 2: Different components of the Finite Element Centered Finite Volume discretization

To get continuous inter-element fluxes, continuity of the pressure and discontinuity of capillary pressure inside the model domain were assumed. An extra system of equations is solved locally on individual NCFVs to get continuous fluxes over the element's faces. The elements are subdivided into sectors by connecting its barycenter to the midpoint of its faces. The flux that exists from one sector of an element enters its other sectors through its facets and these fluxes cancel out. This means that

$$F_{1,2}^{f} = -F_{2,1}^{f} \,, \ F_{2,3}^{f} = -F_{3,2}^{f} \,, \ F_{3,1}^{f} = -F_{1,3}^{f} \tag{3.14}$$

Where $F_{1,2}^{f}$ is the flux from sector 1 to sector 2, $F_{2,1}^{f}$ from sector 2 to sector 1 and so forth (Figure 2). So the total element fluxes can be calculated as:

$$F_{1}^{e} = 0.5(F_{2R}^{s} + F_{3L}^{s}) \,, \ F_{2}^{e} = 0.5(F_{3R}^{s} + F_{1L}^{s)} \,, \ F_{3}^{e} = 0.5(F_{1R}^{s} + F_{2L}^{s}) \tag{3.15}$$
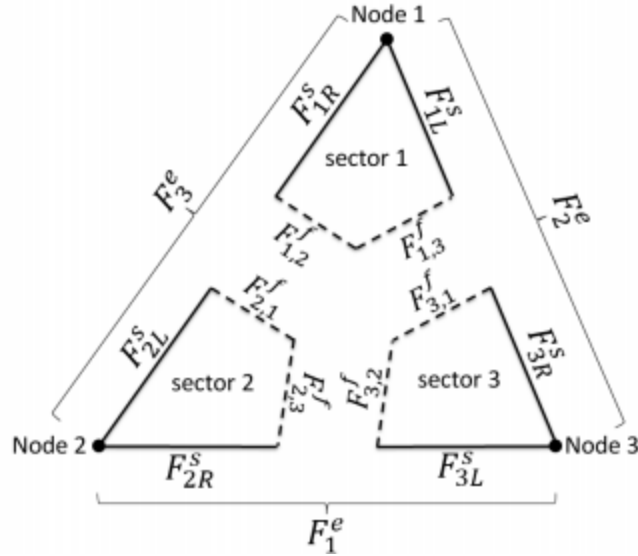
15

Figure 3: Element subdivision into sectors and faces and numbering of transfer terms

3.2. Improved IMPES Implementation

IMPES method has been developed by Stone and Garder (1961). It is very widely used in reservoir simulation particularly for modeling incompressible and slightly compressible fluids. In this method, pressure is solved implicitly while saturation is solved explicitly. In the classical IMPES method, saturation is solved at the previous time step, so this method suffers from serious restrictions regarding the time step size in order to achieve stability.

IMPES spends most of the computational time on calculating the pressure, although usually the pressure field in porous media changes more slowly than that in the saturation field. In CSMP++, improved IMPES method is used to calculate both pressure and saturation. This method was introduced by Chen and Huan (2004). The total velocity field is taken as valid for a larger amount of time, and saturation transport is handled with a smaller time step size on the frozen total velocity field (Bazr-Afkan, 2012).

3.3. Active Element Concept (AEC)

The Active Elements Concept restricts computations to only those elements that suffer from saturation changes and by this saving computational time. This approach cannot be used for the pressure equation and is just suitable for saturation equation (transport equation) which is a hyperbolic equation. Additionally, the speed of the information transfer is finite, so changes in one part of the region do not affect another part of the region.

16

Pressure diffusion is then solved for the entire model and the saturation is solved just for those parts where saturation is changing.

In the reconstructed inter- element velocity field, the elements which are suffering from change in saturation are determined by carrying out a transport step. These are stored as 'active elements'. Faces which are shared by two active elements are 'active faces' and saturation calculation is performed over these, while faces that are between active and inactive elements are 'monitoring faces' and these are excluded from the calculation. The rest of the faces stay inactive. Monitoring faces are actually limiting the flux until it reaches some threshold value (which is defined by the user as activation). The monitoring faces are checked after every transport step, if the flux exceeds the thereshold value, the neighbor element is activated and the monitoring face then becomes an active face. In the same fashion, the deactivation step is done. However, deactivation is a very time consuming process, because it requires a search through all active elements and has to reconstruct the active elements vector afterwards. Therefore deactivation needs to be researched for each individual model depending on its saturation evolution.

Advantages of AEC are:

1. Speeding up the simulation because calculations are restricted to the smaller sections of the model.
2. There is no accumulation of the round off and truncated errors in the inactive parts of the domain.
3. Time step size is restricted by the highest CFL (Courant-Friedrichs-Lewy condition) number in the entire model because saturation transport is done explicitly. Time step size is only restricted by the highest CFL number in the active elements. This means that it is possible to use larger time step sizes.

Since numerical dispersion (which is not wanted in this case) is usually high, for example in first order schemes, by choosing the right flux threshold for activating elements, it is possible to reduce its influence. The use of Welge's approach (1952) is widely used for calculation of the saturation front and then these values are used as activation criterion to ignore numerical dispersion (Bazr-Afkan, 2012).

3.4. CMG governing equations

Conservation of water in the matrix sub-block k:

$$T^x_{wm_{k-1/2}}(p_{wm_{k-1}}{}^{n+1} - p_{wm_k}{}^{n+1}) + T_{wm_{k+1/2}}(p_{w_y}{}^{n+1} - p_{wm_k}{}^{n+1}) - \frac{V_{b_k}}{\Delta t}\left[\left(\frac{\Phi S_w}{B_w}\right)_{m_k}^{n+1} - \left(\frac{\Phi S_w}{Bw}\right)_{m_k}^{n+1}\right] = 0$$

(3.16)

Conservation of oil in the matrix sub-block k:

$$T^x_{om_{k-1/2}}(p_{om_{k-1}}{}^{n+1} - p_{om_k}{}^{n+1}) + T_{om_{k+1/2}}(p_{o_y}{}^{n+1} - p_{om_k}{}^{n+1}) - \frac{V_{b_x}}{\Delta t}\left[\left(\frac{\Phi S_o}{B_o}\right)_{m_k}^{n+1} - \left(\frac{\Phi S_o}{B_o}\right)_{m_k}^{n+1}\right] = 0$$

(3.17)

The equations 3.16 and 3.17 are discretized into finite-difference form using first order backward differences in time, and central differences in space with upstream mobility (User's Guide IMEX, Version 2013.)

4.   Methodology

In the methodology section, 2D models for the comparison will be discussed. Two different 2D models are used in this comparison, test model and Chieberg model. Test model is very simple model which is used as a reference point, and Chienberg model is taken from the literature (Butscher, 2011).

4.1. Test model for CSMP Simulation

To be able to compare geologically complex model in two different simulators, the test model is built in Rhinoceros, then meshed in ICEM CFD and in the end exported as a binary model into CSMP++. The test model will represent the reference point for the comparison.

2D cross-sectional model is 1400 m long and 400 m high, containing just one layer of sand, whose properties are shown in the Table 4.

There are no faults in the model. Injector is on the left side, and producer on the right side, as shown in the Figure 4.
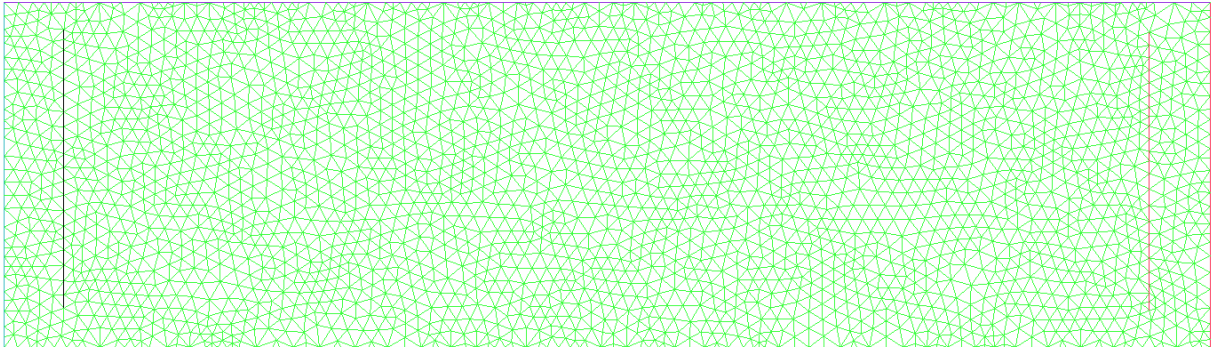
Figure 4: Test model for CSMP simulation

4.2. Test model for CMG simulation

The model for CMG simulation is built directly in CMG, inserting an orthogonal grid. There is just one layer of the sand, the model is homogeneous (1400 × 400 m) with two wells, the left one is injector and the right one is producer. Figure 5 shows the test model for CMG simulation.
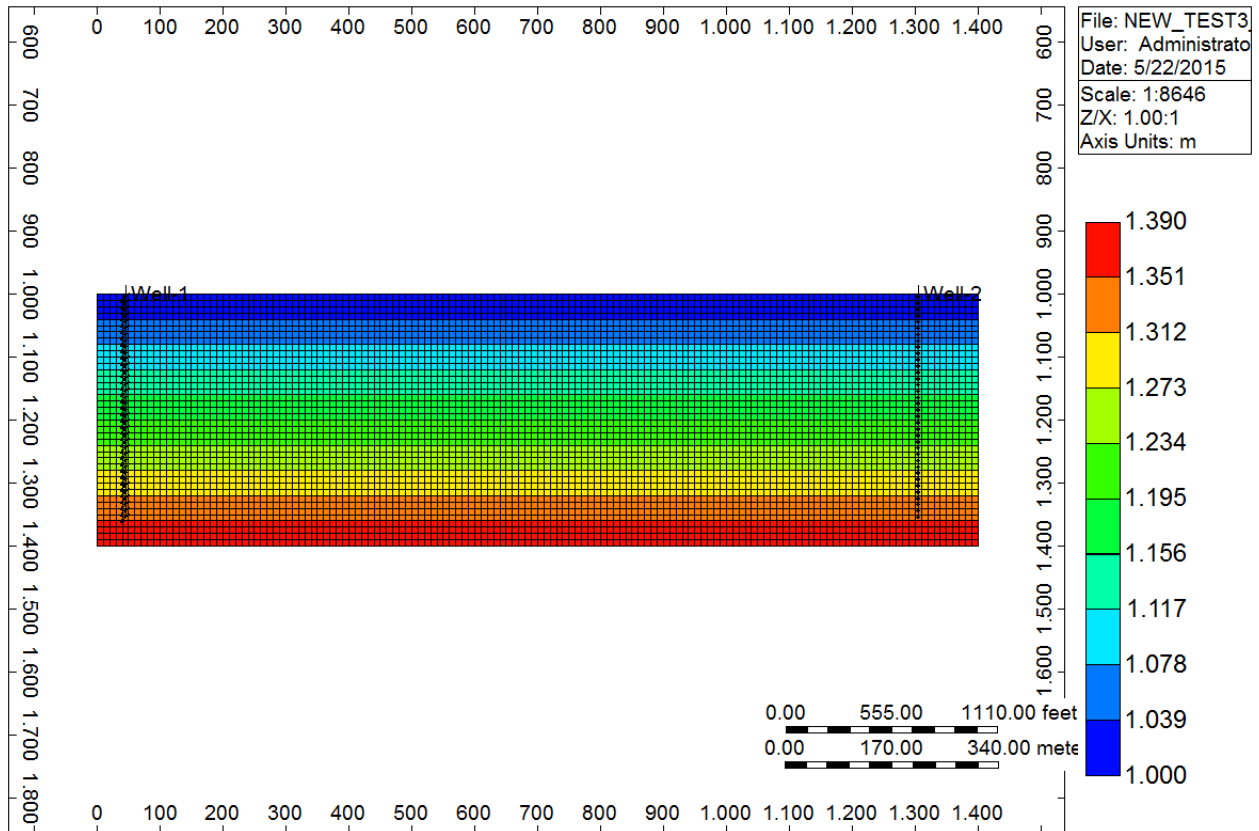

Figure 5: Test model for CMG simulation

4.3. Chienberg model for CSMP++ simulation

This model is based on a cross-sectional area near Chienberg tunnel, Switzerland (Buscher, 2011) (Figure 6).
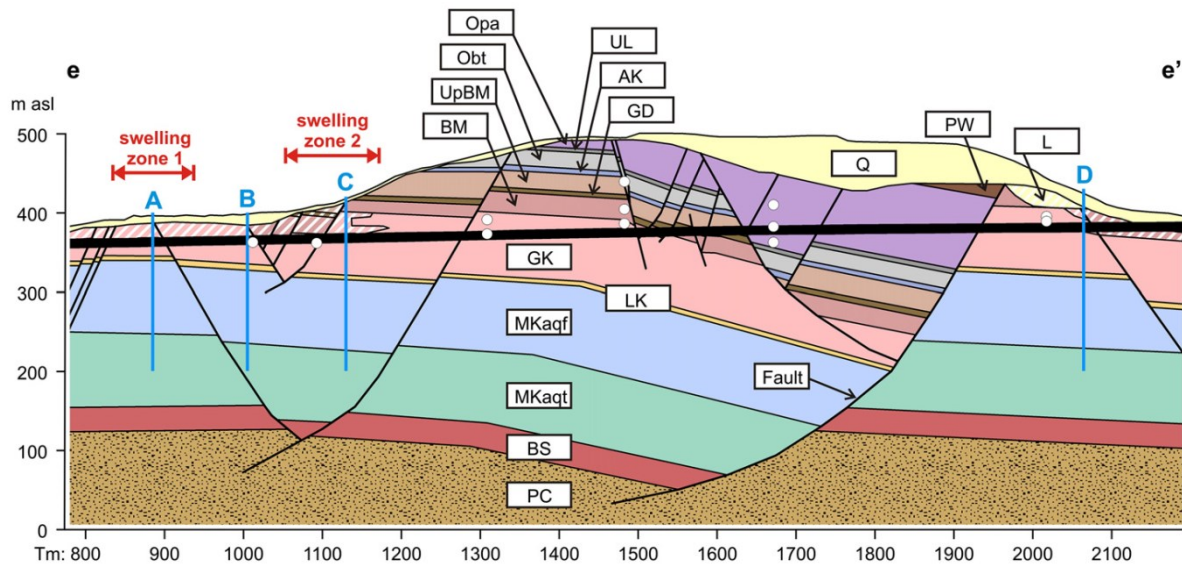
Figure 6: Longitudinal cross-section of the area near Chienberg tunnel, Switzerland (Butscher, 2011)

Figure 7 shows stratigraphy of the model with hydrogeological characteristics of the area.
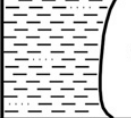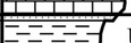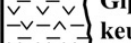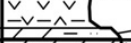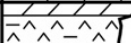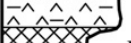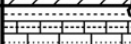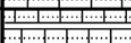
Stratigraphy			Lithology	Lithological description	Thickness (~m)	Aquifer / Aquitard
Quaternary				Fluvio-glacial gravels and sands		Pore aquifer
Jurassic	Dogger	Aalénien	Opa	Monotonous sequence of silty, micaceous clays	95	
	Lias		UL / Obt / AK	Bioclastic limestones, sandy shales	5 / 20 / 5	Low permeability rocks with local aquifers
Triassic	Keuper	Upper	UpBM / GD / BM	Variegated marls, dolomite variegated sandstone	25 / 5 / 25	
		Middle	Gips-keuper	Alternation of shales, nodular and bedded gypsum/anhydrite	80	
		Lower	LK	Porous dolomite and shales	5	
	Muschelkalk	Upper	MKaqf	Porous dolomite / Limestones, bedded	90	Upper Muschel-kalk aquifer
		Middle	MKaqt	Dolomite, laminated / Alternation of shales, bedded and massiv anhydrite / Rock salt beds / Alternation of shales, bedded and massiv anhydrite	80	
		Lower		Dolomite, dolomitic marl and shales	10	
	Bunt-Sst.	Upper	Röt (clay) / Laminated sandstone		10	Intermediate permeabilities
		Middle / Lower	BS	Siliceous sandstone	20	
Permo-Carboniferous			PC	Clastic sedimentary rocks		

Figure 7: Schematic, stratigraphic section also showing hydrogeological characteristics of the study area (Butscher, 2011)

4.4. Geological representation of the Chienberg model

As it can be seen from the Figure 8 the stratigraphic section of the model consists of Triassic and Jurassic rock. **Quaternary** is at the top (the youngest strata) and it consists of fluvio glacial coarse sandstone. Jurassic strata is about 95 meters thick and consists of 4 different types of rocks: **Opalinus Clay, Upper Lias, Obtosus Clay and Arietenkalk (Limestone)**. All of these 4 layers consist of mud, and represent a barrier to flow.

Triassic strata is consists of 3 types of rock: Buntsandstein, Muschelkalk and Keuper. **Buntsandstein (Bunter)** is colored sandstone. It is made in a fluvial environment of deposition and consists of coarse grained red sandstone. For that reason, it is chosen to be reservoir layer, as it has the best qualities concerning permeability, porosity and sorting.

Muschelkalk exists as Muschelkalk aquifer and aquitard. **Muschelkalk aquifer (Coquina aquifer)** has better qualities in terms of permeability and porosity, as a reservoir layer. Both of the Muschelkalk rocks are deposited in an arid climate. **Muschelkalk aquitard (Coquina aquitard),** together with Muschlekalk aquifer, is approximately 80 and 90 meters thick, respectively. **Keuper** is made of dolomite, shales or claystones and evaporites which were deposited during the Middle and Late Triassic epochs and usually lies on Muschelkalk. Together, Muschelkalk and Buntsandstein make a Germanic Triass Group (this is a characteristic sequence of Triassic strata).

Permo- Carboniferous is clastic sedimentary rock with intermediate permeability.

There are 19 **faults** in this reservoir cross-section (Figure 6). All faults are normal faults with high permeability, which makes the production from this reservoir easier. The faults are approximately 1 m wide.

The 2D model was built in Rhinoceros and meshed in ICEM CFD. A simulation was then conducted by CSMP.

Figure 8 represents 2D model built for CSMP++ simulation.
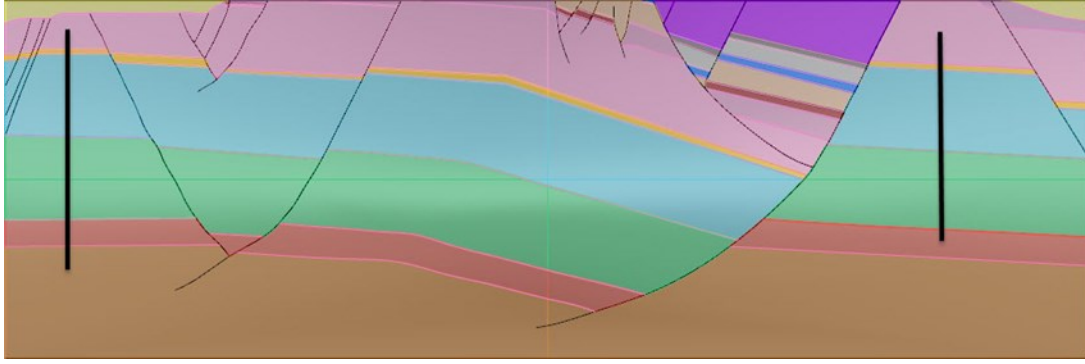
Figure 8: 2D cross section map for CSMP++ water flooding simulation. The area is 1400 × 400 m high

4.5. Chienberg model for CMG simulation

In order to compare two different approaches of discretization, the Finite Difference and the Finite Element Centered Volume approaches, the Chienberg model was built in a SKUA Paradigm and imported to CMG. Figure 9 shows the Chienberg model for CMG simulation.
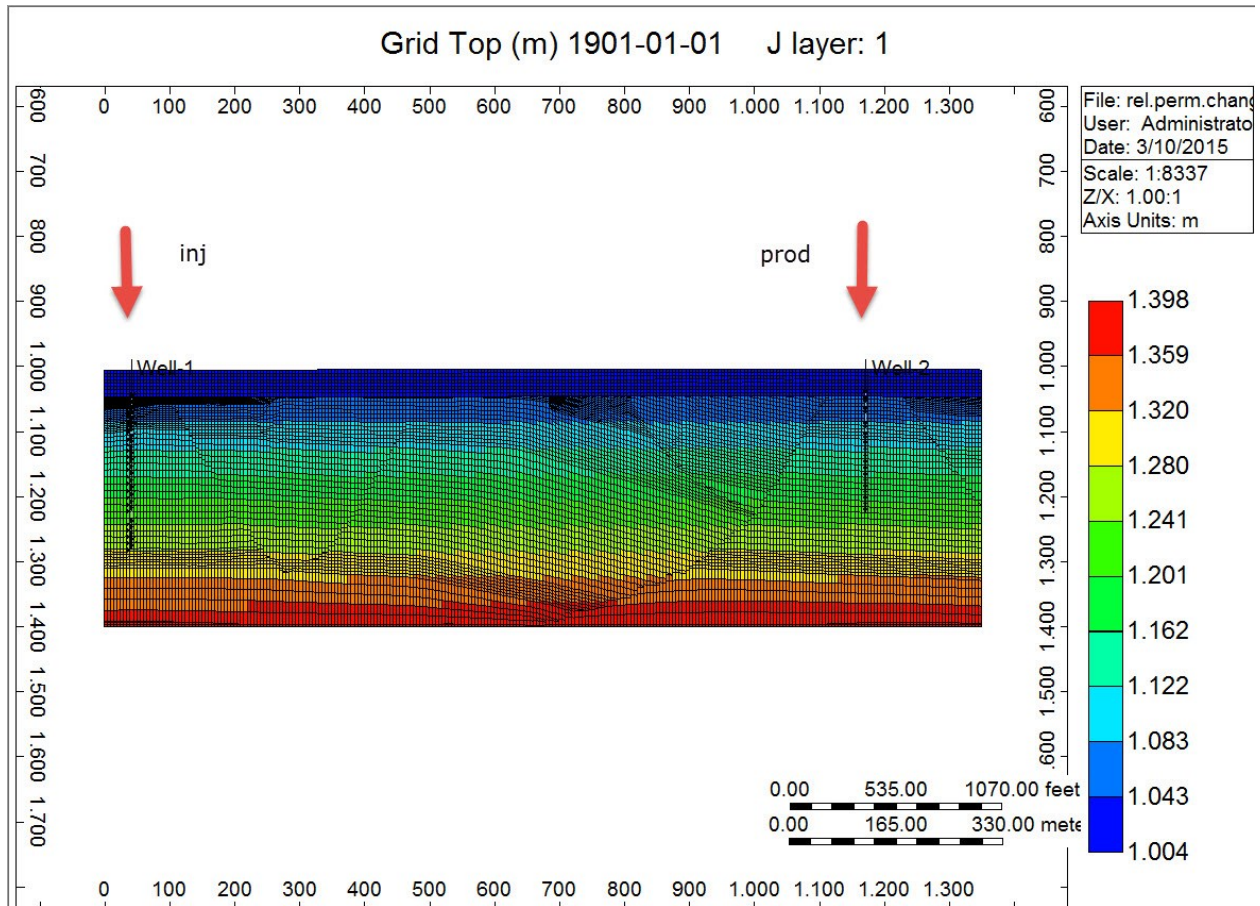
Figure 9: CMG model for water flooding simulation

4.6. Boundary conditions and simulation setup

Boundary conditions and simulation setup are discussed in this chapter, since they are very important in initialization of the models and furthermore simulations. These setup may lead to differences between the results and this will be discussed in the details in the Results section.

Test model

Table 3 shows the initial conditions for CMG simulation. OWC is at the bottom of the model, the same as in the complex model, and the same initial conditions are applied to both models.

Reference pressure (kPa)	9849
Reference depth (m)	1004
OWC (m)	1400

Table 1: Initial conditions for CMG simulation

The wells are perforated through every layer in order to increase injection and production. The radius of the wells is 0.0762 meters (diameter 15 cm). The length of the wells is 320 meters approximately.

Table 4 shows the initial conditions for CSMP simulation. Note that the same initial water saturation, initial oil saturation, permeability and porosity is used in CMG simulator. The Brooks-Corey relative permeability curves for Bunt-sandstein are inserted to CMG simulator.

Rock	Porosity (-)	Permeability (mD)	Entry pressure (Pa)	Swr (-)	Sor (-)	Swi (-)	Soi (-)	λ (-)
Bunt sandstein	0,22	182	3389	0,19	0,15	0,19	0,81	2,35

Table 2: Initial conditions for CSMP simulation

Boundary conditions:

1) CASE 1

CSMP simulation

No-flow boundary condition at the TOP, LEFT, RIGHT, at the BOTTOM Dirichlet pressure of 13.73 MPa, injecting and producing with fluid sources of 1.31e-6 m^3/m^3s. Volume modifier is set to 0.0176 to account for the diameter of the wells (0.15 m).

CMG simulation

No-flow boundary condition at the TOP, LEFT, RIGHT, at the BOTTOM aquifer (Carter-Tracy infinite model), injecting and producing with rates of 28.3 m^3/day. Radius of the aquifer is set to 1400 m. Porosity and permeability are left as default (they are averaged).

2) CASE 2

CSMP simulation

No-flow boundary conditions, injecting with the water volume source of 1.31e-6 m^3/m^3s, producing with the bottom-hole pressure of 1MPa. Volume modifier set to 0.0176 to account for the well diameter (0.15 m).

CMG simulation

No-flow boundary conditions, injecting with the water volume source of 28.3 m^3/day, producing with the bottom hole pressure of 1MPa.

Chienberg model

Initial conditions for FD simulation are shown in Table 8. The reservoir initially contains water and oil (two-phase flow, incompressible, and immiscible).

<div align="center">

Table 8: Initial condition for simulation with FD approach

Reference pressure (kPa)	9849
Reference depth (m)	1004
OWC (m)	1400

</div>

The wells' diameter is the same as in the test case. The length of the wells is 250 meters.

Initial conditions for FECFV simulation are shown in Table 9.

<div align="center">

Table 9: Initial conditions for simulation with FECFV approach

Rock	Porosity (-)	Permeability (mD)	Entry pressure (Pa)	Swr (-)	Sro (-)	Sw (-)	So (-)	λ (-)
Permo-carboniferous	0.14	18.2	8461	0.15	0.15	0.15	0.85	2.5
Bunt sandstein	0.22	182	3389	0.19	0.15	0.19	0.8	2.35
Muschelkalk aquitard	0.06	18.2	5390	0.1	0.15	0.1	0.9	1.5
Muschelkalk aquifer	0.23	182	3474	0.5	0.15	0.5	0.5	1.5
Gipskeuper	0.06	18.2	5446	0.01	0.15	0.01	0.99	2
Gipskeuper weathered	0.1	18.2	7259	0.06	0.15	0.06	0.94	2
Upper lias	0.1	182	2271	0.13	0.15	0.13	0.87	2
Limestone	0.08	108	2668	0.19	0.15	0.19	0.81	2
Arietenkalk	0.28	182	3818	0.08	0.15	0.08	0.92	2
Bunte mergel	0.11	18.2	7639	0.08	0.15	0.08	0.92	2.5
Upper buntemergel	0.11	18.2	7639	0.08	0.15	0.08	0.92	2
Lettenkeuper	0.16	182	2934	0.15	0.15	0.15	0.85	2.5
Opalinus clay	0.03	0.2	7259	0.01	0.15	0.01	0.99	3
Obtosus clay	0.08	18.2	6685	0.04	0.15	0.04	0.96	2.5
Quaternary	0.24	91.2	4994	0.35	0.15	0.35	0.65	2.35

</div>

The same properties (porosity, permeability, initial water and oil saturation) are used in CMG simulation. All the values are taken from the literature (Rautenbacher, 2013).

CASE 1 is the same case as for the test model.

CASE 2 is as well no-flow boundary conditions, with the difference that it is producing with bottom hole pressure of 1E6 Pa. Injection rate is the same as in the CASE 1.

There is no aquifer at the bottom in CMG, and there is no Dirichlet pressure defined at the bottom in CSMP.

5. Results

Results of the static and dynamic evaluation for test and Chienberg model are discussed in this chapter.

5.1. Test model

The comparison of the test model will be done for the static and dynamic model. As previously explained in the Chapter 2, these two evaluation methods are tightly connected and will be explained in details in this chapter.

5.1.1. Static evaluation

The most important static properties for this comparison are pore volumes, initial oil in place, boundary conditions, and simulation setup.

Pore volumes and initial oil in place

Pore volumes and initial oil in place (OIIP) have been calculated in Excel for simulation with FECFV approach, while CMG simulator (FD approach) outputs it automatically created.

Table 3: Pore volumes and initial oil in place for CSMP simulation

Layer	Ni(m3)	phi ( )	Swi ( )	Vb(m3)	Vv(m3)
Sand	99792,00	0,22	0,19	560000,00	123200,00

Table 4: Calculated properties (OIIP, pore volumes and WIP) for two different approaches

Calculated property		FECFV approach	FD approach
Total Oil in place (m3)		100115	101760
Total Pore Volume (m3)		123200	123200
Water in place (m3)		23731	23400

The difference between calculated oil initial in place 1,62 % which is acceptable difference. Since the incompressible flow needs to be modeled, B_o is approximately 1, and R_s is constant. The problem related to this, is that CMG simulator does not allow for R_s to be constant and neither for B_o to be 1. Both parameters need to increase monotonically, as in compressible fluid flow, so this is making a small differences in results, as it can be seen from the Table 2.

5.1.2. Dynamic evaluation

The comparison of the most important dynamic parameters such as recovery factor, cumulative oil produced, time to breakthrough, pressure distribution, flow velocity distribution are presented in this section.

Recovery factor

Recovery factors of the test model are simulated and compared for 2 different scenarios.

1) CASE 1

Injection rate of 28.3 m3/day is used (converted to the source 1.31E-06 m^3/m^3s by dividing the injection rate by the volume of the well).

Figure 10 shows recovery factor over time: CMG shows linear behavior while CSMP in this case has exponential trend. Difference in total RF is around 16 %. As already mentioned in CSMP++ FECFVM IMPES 2-Phase Flow Simulator Documentation (Matthai, 2012.), it is better to use source term for the injector and Dirichlet fluid pressure for the producer, to avoid the problems related to the balance of the inflow and outflow. This will be later discussed, to explain why it is better to use CASE 2 for the comparison.

Another problem is related to the boundary conditions. Aquifer was specified in CMG in order to try to make the simulation setup the same. This is making the huge differences between the results, since Dirichlet pressure in CSMP at the bottom is fixed pressure, and aquifer behaves as Neumann boundary condition with the changes in the time. The try to specify aquifer at the bottom of the model in CMG was in order to prescribe an aquifer pressure. However, it is only possible to calculate the change in the boundary pressure and this makes it harder to get the same simulation setup in both simulators.
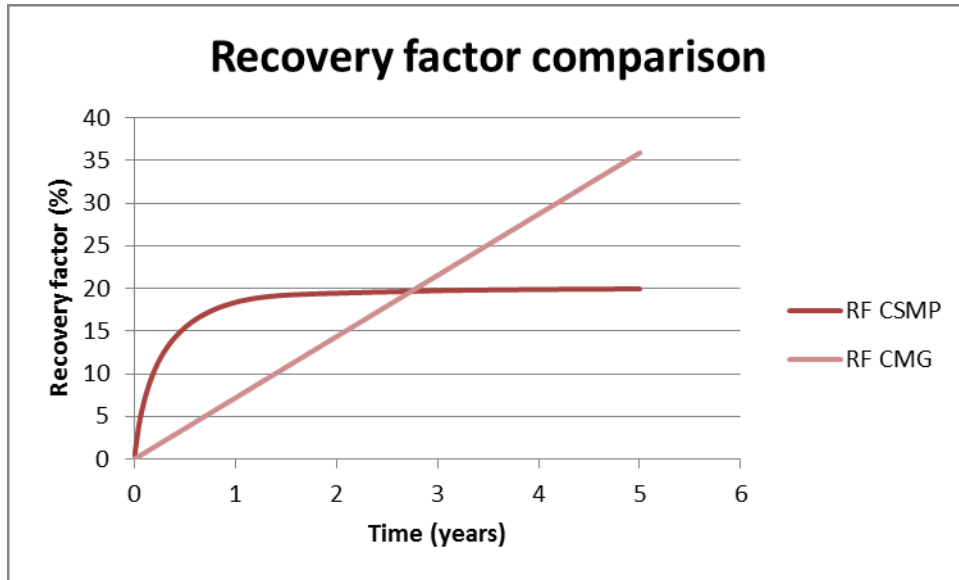
Figure 10: Recovery Factor comparison

2) CASE 2

Injection rate for injector is 28.3 m3/day (1.31.E-06 in terms of the water volume source) and bottom hole producing pressure is 1000 kPa.

Figure 11 shows the difference between the recovery factors of two simulators which is 0.38 % in this case.

Figure 11: Recovery factor comparison

So, these conditions should be used for the comparison of the complex model.

However, both case will be used for the comparison, in order to examine behavior and differences between the reservoir simulators.

Time to breakthrough

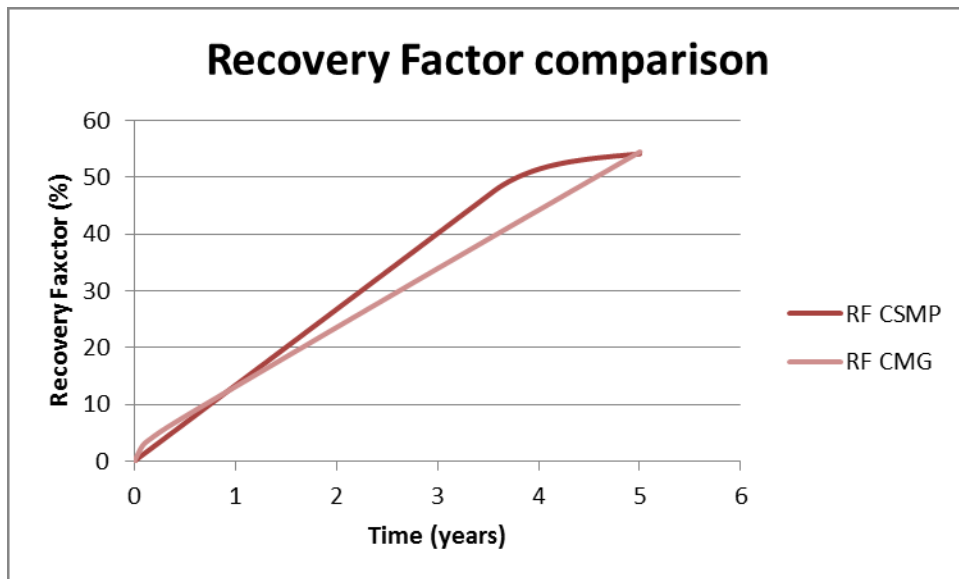Time to breakthrough and water cut are calculated and plotted for test model for two different simulation scenarios.

1) CASE 1

Both simulators show the same behavior regarding the water cut, the water cut was 0, and this is also obvious from the Figures 17 and 18 which show the saturation fronts (front did not advance enough to the producer).

2) CASE 2

Figure 12 shows that water breakthrough happens after 5 years in CMG. On the contrary, in CSMP++ it happens after 3,6 years (Figure 12). Nevertheless, this water cut is very low. This behavior can be explained by the oil saturation front which in CSMP advances faster than CMG.
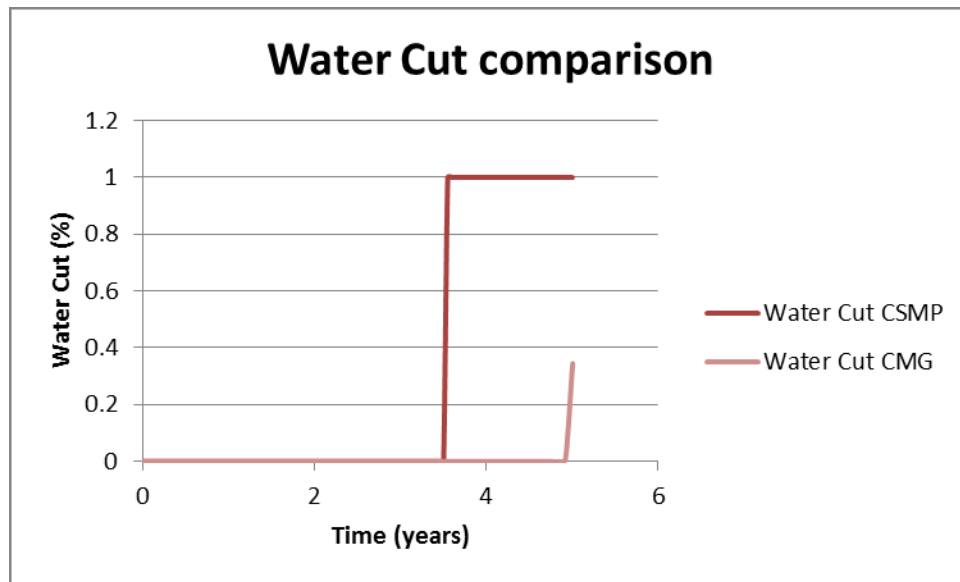
Figure 12: Water Cut comparison between the CSMP and CMG simulation

Cumulative oil production

Cumulative oil produced is compared for test model for two different simulation scenarios.

1) CASE 1

Figure 13 shows the cumulative oil produced for both simulators. CMG and CSMP show different behavior like recovery factors. Difference in cumulative oil produced at the end of the simulation is around 58%.
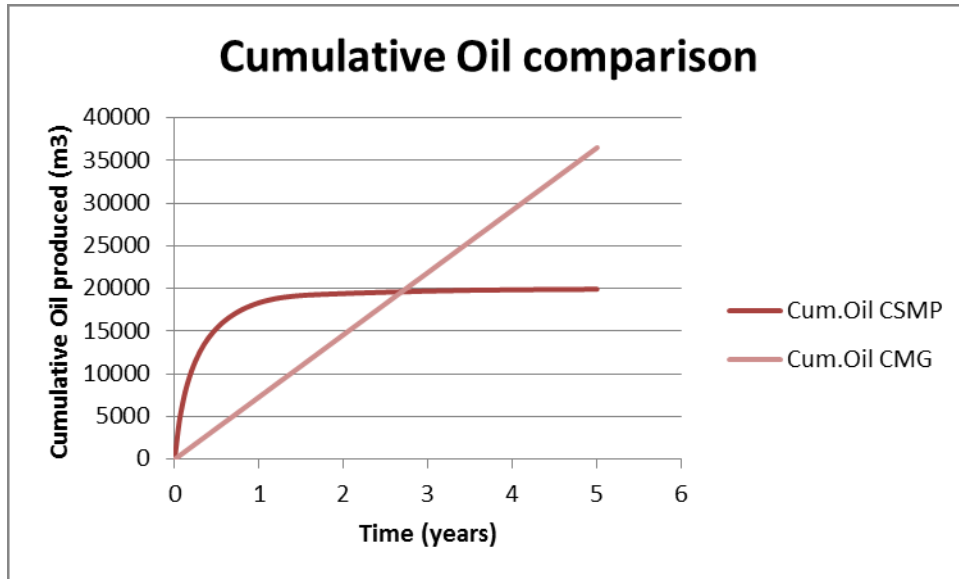
Figure 13: Cumulative Oil produced comparison

2) CASE 2

Figure 14 shows the comparison of the cumulative oil produced between the simulators. The difference is around 2.64%, which shows better agreement in comparison to the no-flow boundary conditions (in CSMP Dirichlet pressure at the bottom, in CMG aquifer is defined at the bottom).
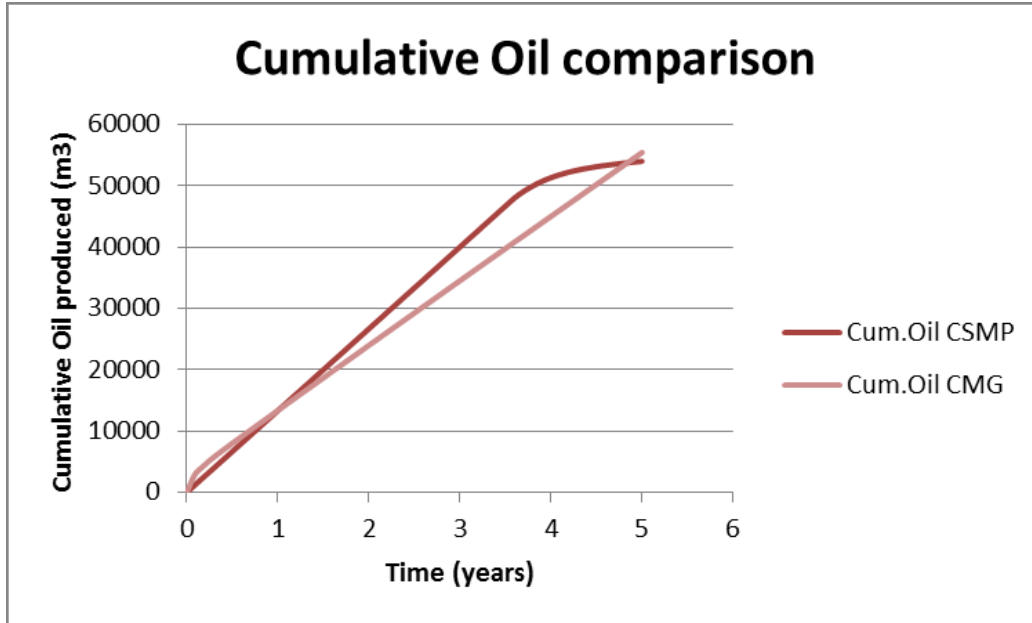

Figure 14: Comparison of the cumulative oil production between CSMP and CMG simulators

Flow velocity distributions

Flow velocity distributions are compared together with the oil saturation front and fluid distribution for two different scenarios.

1) CASE 1
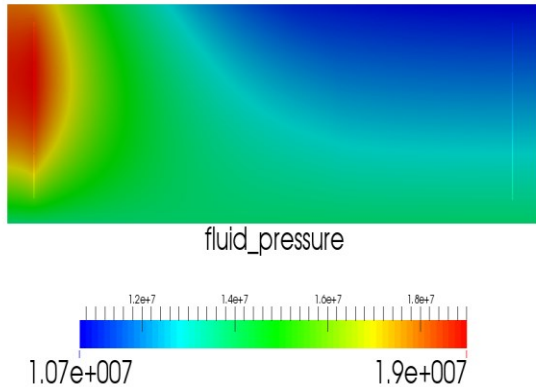
Figure 15: Pressure distribution after 5 years in CSMP in Pa
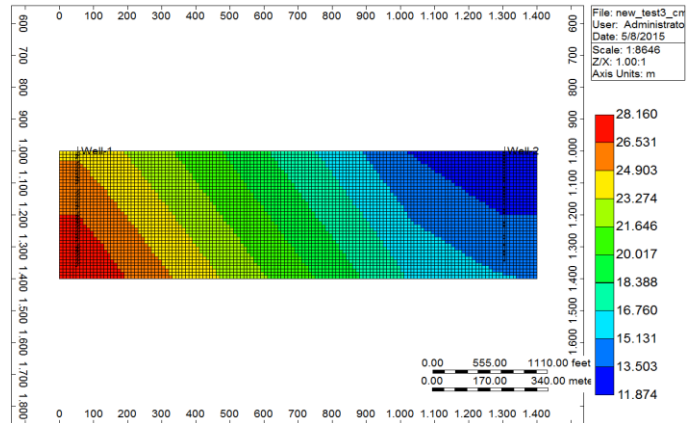
Figure 16: Pressure distribution after 5 years in CMG in kPa

Pressure distributions (Figure 15 and 16**Figure 16**) show completely different profile: in CSMP the highest pressure is around injector, but transition zone from the injector to the producer looks not well sorted as in CMG simulator. Maximum pressure at the injector in CSMP is 190 bar, at the opposite, in CMG is 281 bar. Minimum pressure at the producer in CSMP is 107 bar and in CMG 118 bar. The values of the pressure are not so different, but the difference in fluid pressure distribution is obvious. This is due to the different simulations setup for CASE 1. Dirichlet fixed pressure at the bottom boundary in CSMP produces different results compared to the Aquifer defined at the bottom in CMG.

Figures 17 and 18 show that oil saturation front is faster in CMG, which is logical, since the pressure is higher in CMG. Nevertheless, in both simulators oil saturation front do not arrive to the producer so as previously mentioned, it is obvious that there is no water breakthrough. Both simulators show water inflow from the bottom boundary.
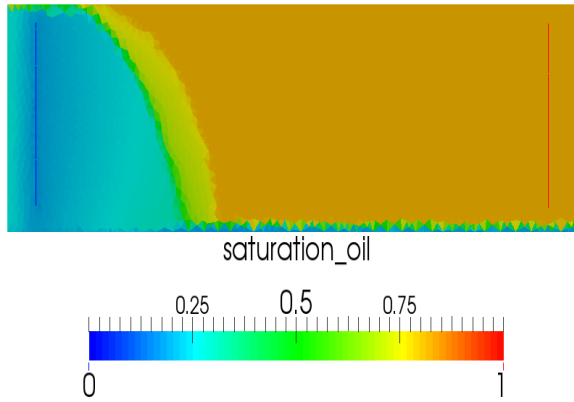
Figure 17: Oil saturation front after 5 years in CSMP
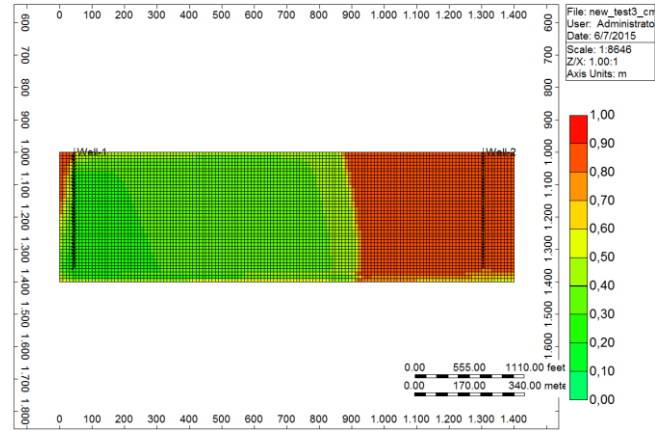
Figure 18: Oil saturation front after 5 years in CMG

Figure 19, 20 and 21 show a big difference between the flow velocities. The magnitudes in CMG are much lower than CSMP. Figures 19 and 20 show the velocities around the injector and producer, with the minimum velocity of 1E-05 m/s and the maximum of 8.74E-05 m/s (which is approximately equal to min. of 0.864 m/day and 7.5 m/day). Figure 22 shows the velocities in CMG simulator with the minimum of -0.038 m/day and maximum of 0.121 m/day. Note that the Figure 22 shows the oil velocity in x direction. This is the reason why velocities at the left of the injector and at the right of the producer are negative.

Figure 19: Oil velocity near injector after 1 month in CSMP

Figure 20: Oil velocity near producer after 1 month in CSMP

Figure 21: Oil velocity distribution after 1 month in CMG

2) CASE 2

Figures 22 and 23 show good agreement between the results regarding the oil saturation front.
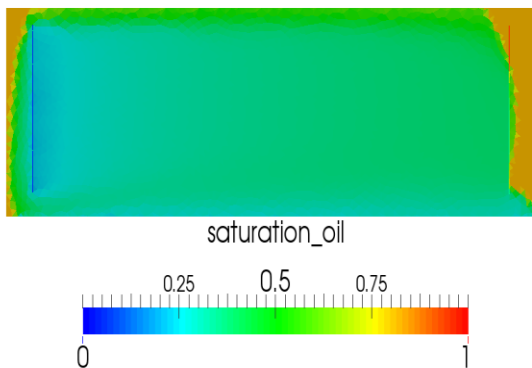
Figure 22: Oil saturation front after 5 years in CSMP
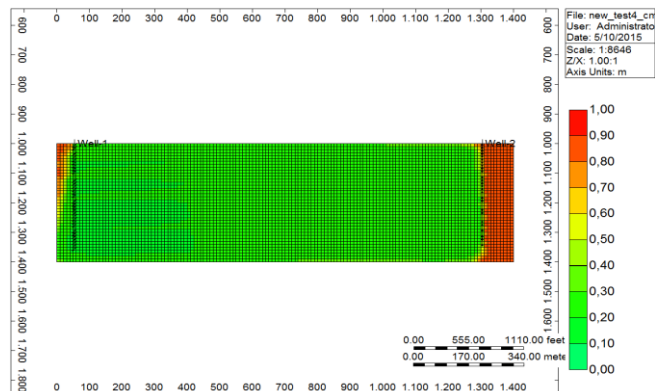
Figure 23: Oil saturation front after 5 years in CMG

Figures 24 and 25 show better agreement between simulators regarding the pressure distribution, compared to the case 1.
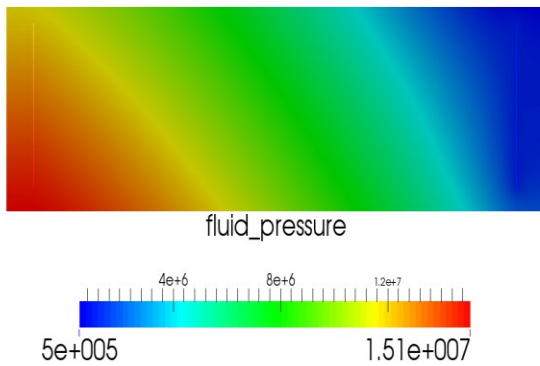
Figure 24: Pressure distribution after 5 years in CSMP in Pa
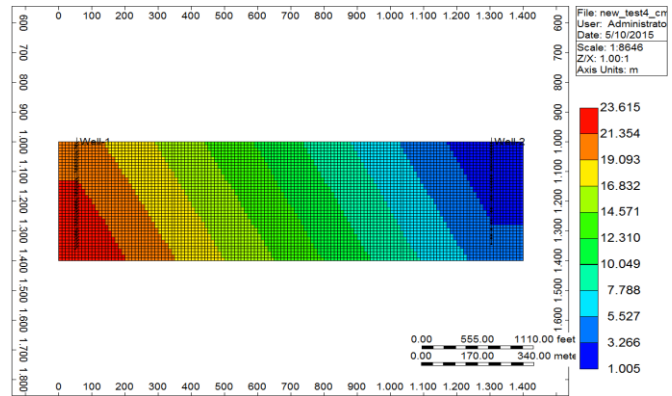
Figure 25: Pressure distribution after 5 years in CMG in kPa

Figure 26, 27 and 28 show oil velocity distributions in CSMP and CMG. Minimum velocity in CSMP simulator is 1E-06 m/s and maximum 3.95e-06 m/s (which is approximately 0.0862 m/day and 0.341 m/day). In CMG oil velocities range from -0.062 m/day to 0.168 m/day. As already mentioned, oil velocities are shown in x direction (this is the reason for negative oil velocities).
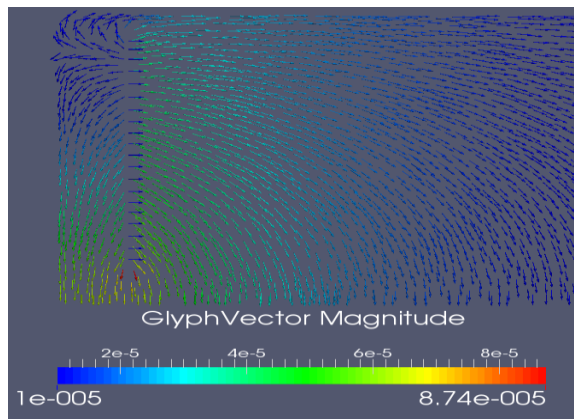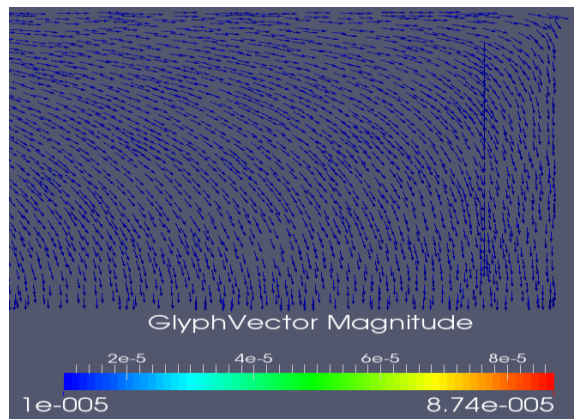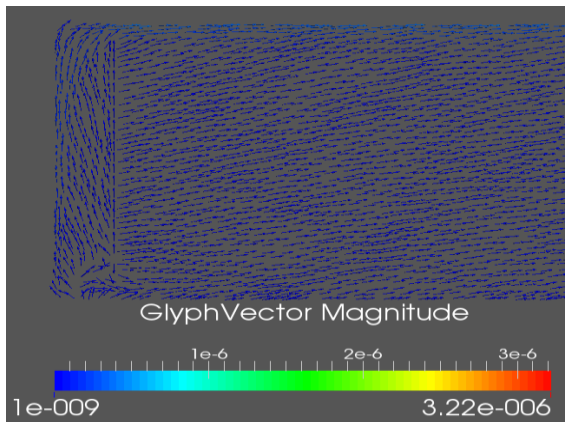

Figure 26: Oil velocity near injector after 1 month in CSMP
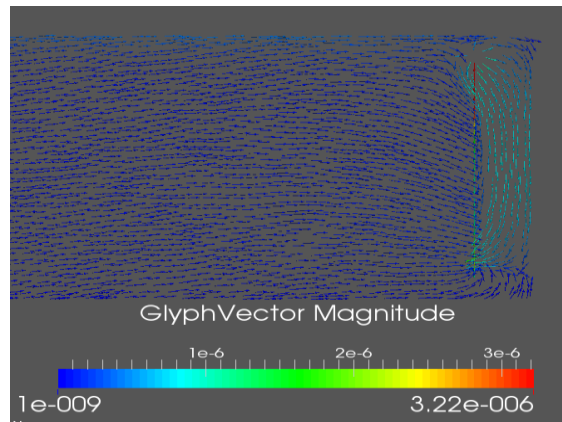
Figure 27: Oil velocity near producer after 1 month in CSMP
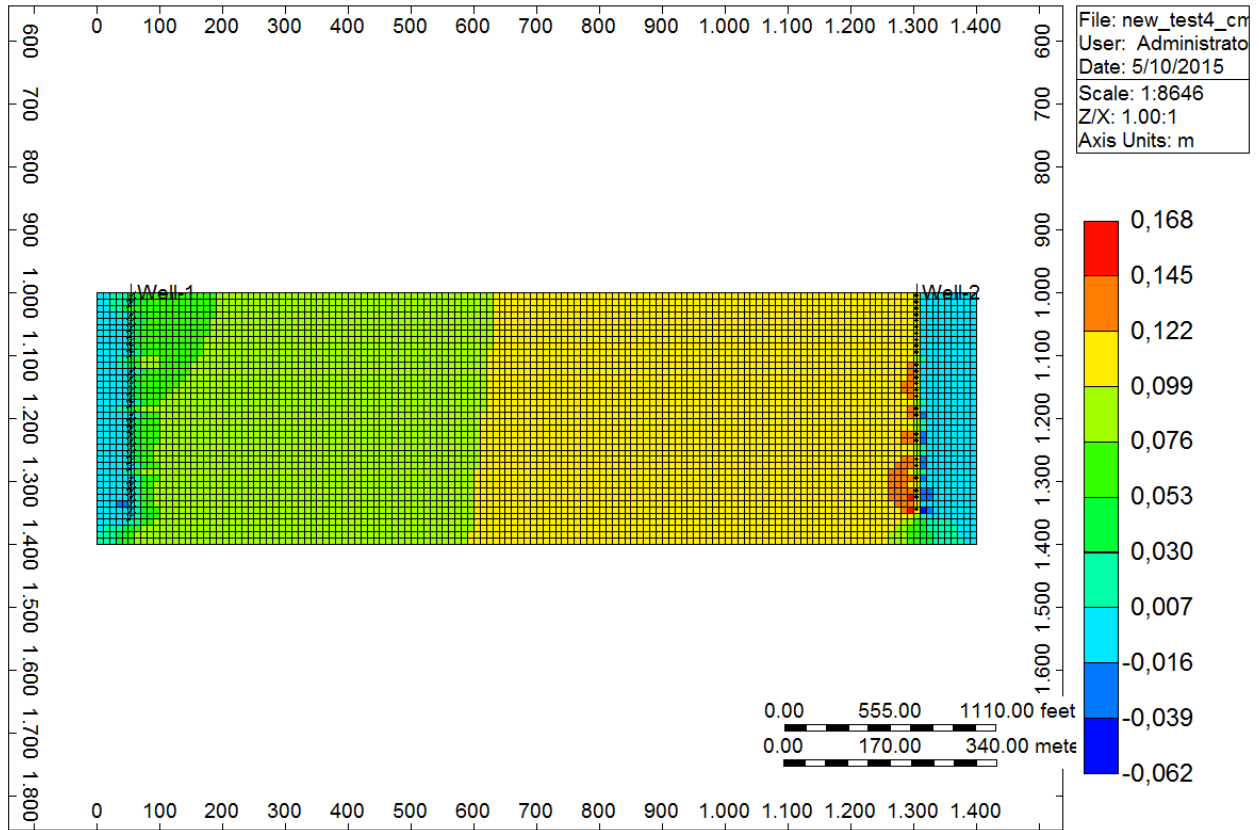
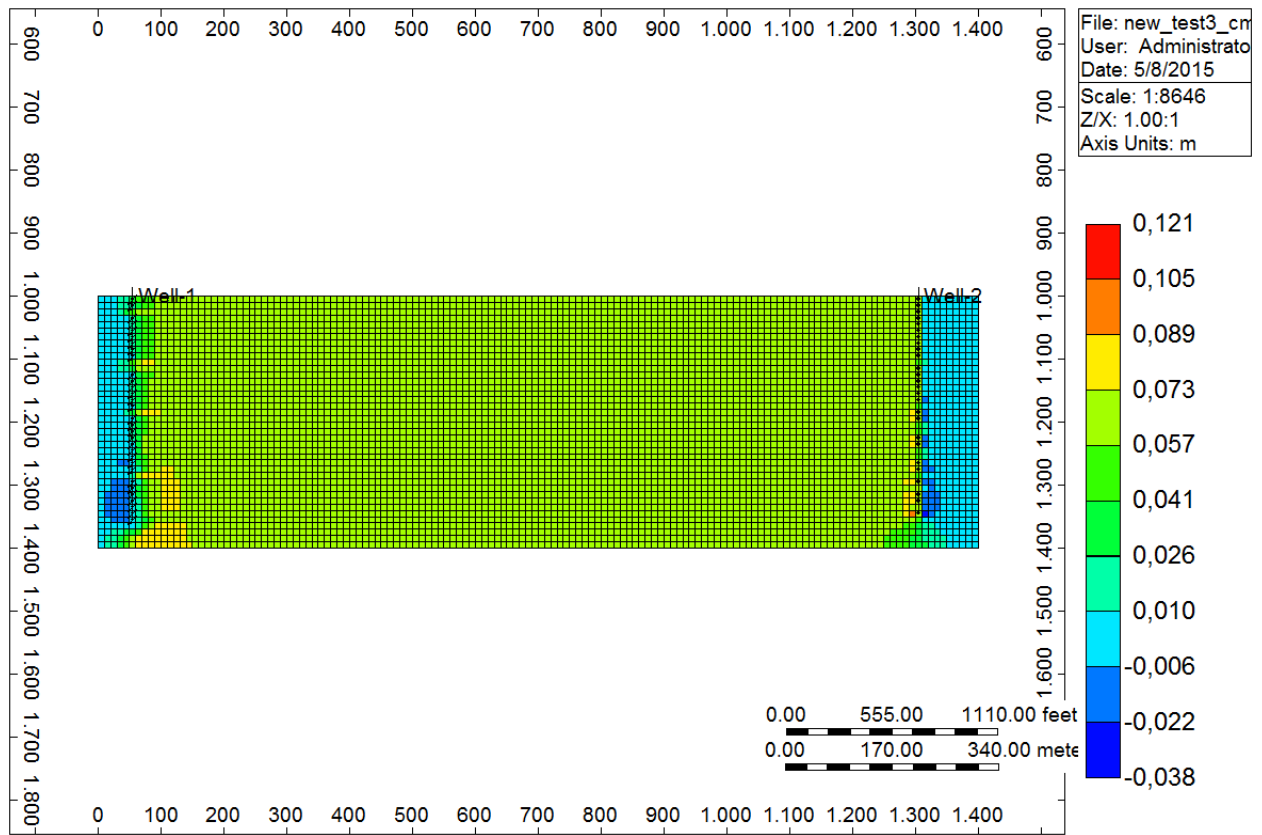**Figure 28: Oil velocity distribution after 1 month in CMG**

Compared to the case 1, the case with fixed bottom-hole pressure show better agreement in terms of the oil velocities as well as pressure distribution, recovery factors and cumulative oil produced.

5.2. Chienberg model

The same comparison as for the test model will be made for the complex model.

5.2.1. Static evaluation

The most important static evaluation parameters such as pore volumes and initial oil in place are compared in this chapter.

Pore volumes and initial oil in place

The following table shows the calculated oil initially in place and pore volumes for the CSMP++ simulation.

Table 5: Calculated OIIP and pore volumes for simulation with FECFV approach

| Layer	Ni(m3)	phi ( )	Swi ( )	Vb(m3)	Vv(m3)
Arietenkalk	428.60	0.28	0.11	1719.90	481.57
Buntsandstein	6723.08	0.22	0.2	38199.32	8403.85
Limestone	147.95	0.08	0.13	2125.69	170.06
Gipskeuper	4404.83	0.06	0.15	86369.22	5182.15
Lettenkeuper	1188.82	0.16	0.15	8741.32	1398.61
Permo carboniferous	12480.20	0.14	0.15	104875.63	14682.59
Quaternary	1239.03	0.24	0.35	7942.50	1906.20
Bunte mergel	604.07	0.11	0.08	5969.03	656.59
Upper buntemergel	618.07	0.11	0.08	6107.36	671.81
Upper lias	150.37	0.1	0.1	1670.73	167.07
Obtosus clay	309.19	0.08	0.16	4601.09	368.09
Opalinus clay	399.70	0.03	0.16	15861.27	475.84
Muschelkalk aquifer	22134.10	0.23	0.54	209206.99	48117.61
Muschelkalk aquitard	5394.59	0.06	0.1	99899.81	5993.99
Gipskeuper weathered	203.40	0.1	0.06	2163.80	216.38
SUM	56425.99			595453.7	88892.41

The table shows OIIP and pore volumes for each layer and the sum of all layers, which gives the total OIIP and pore volumes. Ni is initial oil in place (given in the output of the simulator), phi is the porosity of the particular layer, Swi is initial water saturation, Vb is bulk volume, Vv is pore volume.

Output from CMG shows the value of 54950 m^3 for OIIP while for CSMP it is 56426 m^3. This makes a difference of 2.5% between them.

Differences between the two approaches can be caused by different Bo and Rs, as previously mentioned and this has a big influence on the oil recovery and oil produced which will be shown later. Table 6 shows the calculated properties for two different approaches.

Table 6: Calculated properties (OIIP and pore volumes) for two different approaches

Calculated property	FECFV approach	FD approach
Total Oil in place (m3)	56426	54950
Total Pore Volume (m3)	88892	73323
Water in Place (m3)	20185	17365

For calculation of OIIP and pore volumes, B_o and R_s are two parameters which play a major role. Since the incompressible flow is modeled, Bo should tend to be 1 and Rs is constant (33scf/stb). Viscosities and bubble point pressure are taken from the literature (Rautenbacher, 2013.). Summary of the fluid properties used is shown in the Table 7.

Table 7: Fluid properties used in the simulations

Property	Value
Tres (°C)	52
pb (bar)	11.3
Oil density (kg/m3)	802
Oil viscosity (cP)	1.7
Oil API Gravity (°)	45
Oil Specific Gravity (-)	0.8
GOR (scf/STB)	33
Bo (-)	1
Water density (kg/m3)	989
Water viscosity (cP)	0.5
Geothermal gradient (°C/100m)	3

5.2.2. Dynamic evaluation

Dynamic parameters (recovery factor, cumulative oil production, fluid pressure, oil saturation distribution and fluid velocity distributions) are discussed in this chapter.

Recovery factor

Recovery factor is considered for two cases.

1) CASE 1

The recovery factor showed the difference of 8% in the results of the two simulators. Figure 29 shows a recovery factor of 58% and 50% after 5 years of simulation in the CMG and CSMP simulators respectively. Note that initial conditions, OWC and injection rates, as well as relative permeability curves and rock properties are the same in both simulators.
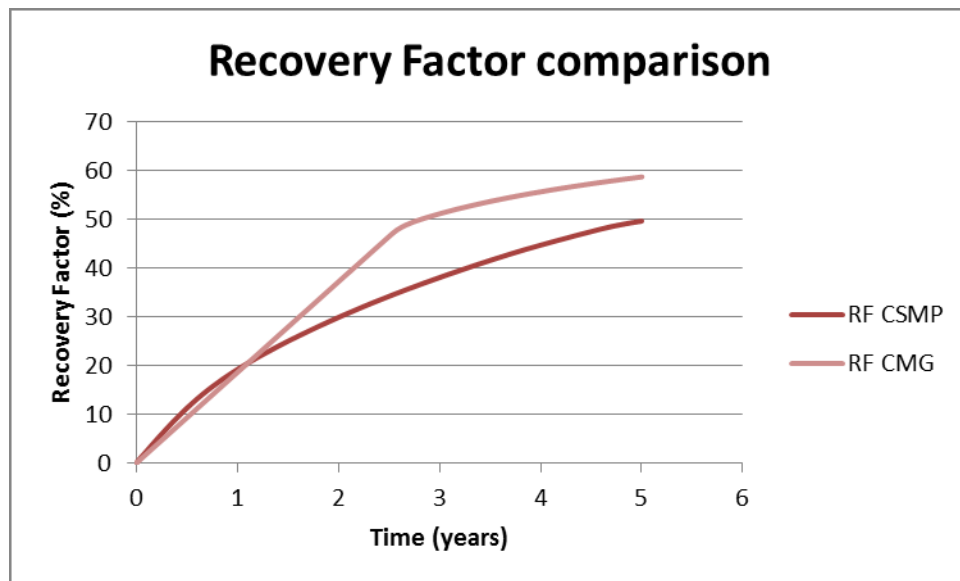

Figure 29: Recovery factor comparison between CSMP and CMG simulation

2) CASE 2

Figure 30 shows approximately 9% difference between CMG and CSMP predictions for recovery factor, which is 49 % for CMG and 40 % for CSMP.
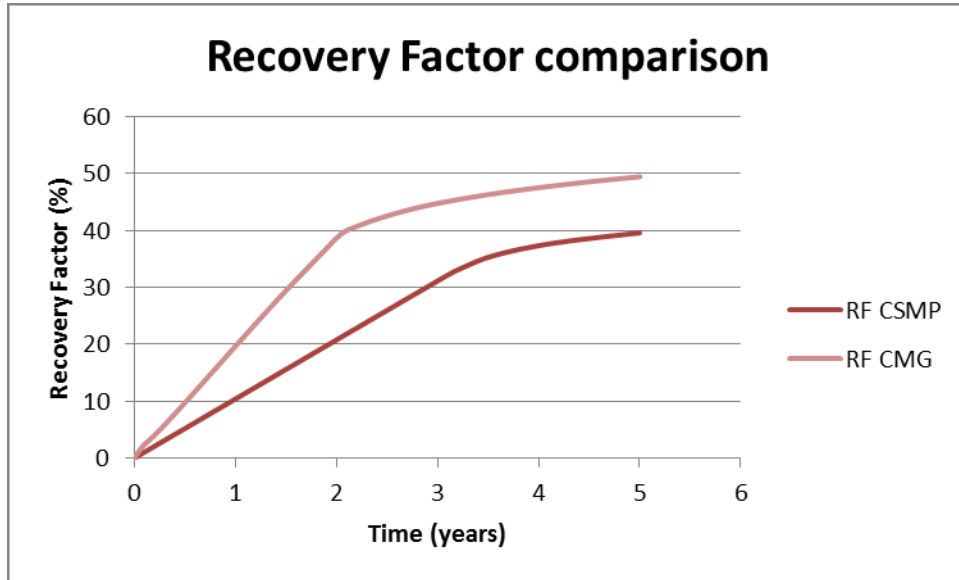
Figure 30: Recovery factor comparison between CSMP and CMG simulation

Time to breakthrough

Time to breakthrough is observed for two cases.

1) CASE 1

From the Figure 31, it can be concluded that the water breakthrough happens faster in CSMP, after approximately 7 months of production (when water in place (WIP) in well 2 (producer) starts to rise), while this happens after 1.6 years in CMG. The reason why water breakthrough happens faster in CSMP simulation is because the oil saturation from the bottom approaches faster to the production well than in CMG. It is obvious that water coning, formed around Well 2 (producer) influences also faster water breakthrough. This instability is not observed in CMG.

Nevertheless, water cut stays very small until the end of the simulation in both simulators.
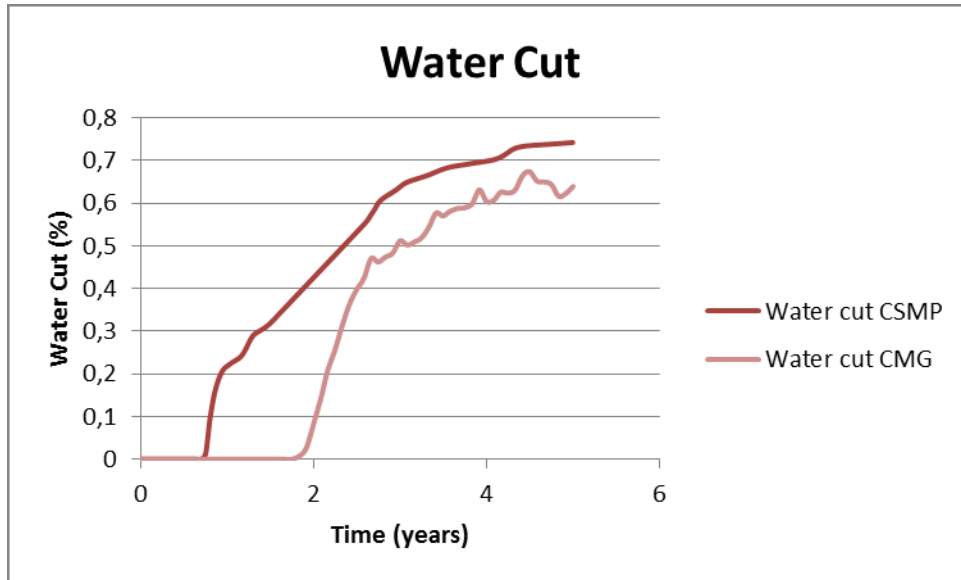
Figure 31: Water Cut comparison between CSMP and CMG simulation

2) CASE 2

Figure 32 shows that water breakthrough happens faster in CSMP, after approximately 1.2 years. In CMG this happens after 2.2 years. Additionally, it can be observed that CSMP simulation, after approximately 2 years, has constant water cut, while water cut in CMG increases. However, water cuts in both simulations are pretty small, which makes water production problems easier to handle.

Figure 32: Water cut comparison between CSMP and CMG simulation

Grid resolution to express instabilities

As previously said in Chapter 2, grid resolution plays a great role in representing the reservoir in a realistic way. This chapter explains the differences between the grid resolution of the model for CSMP++ and CMG models.

As mentioned in the Chapter 4, the model for CMG is modeled in the SKUA Paradigm and then exported to CMG. The grid of the CMG model is structured grid and in Figure 9, it can be seen, that this structured grid is built from many rectangula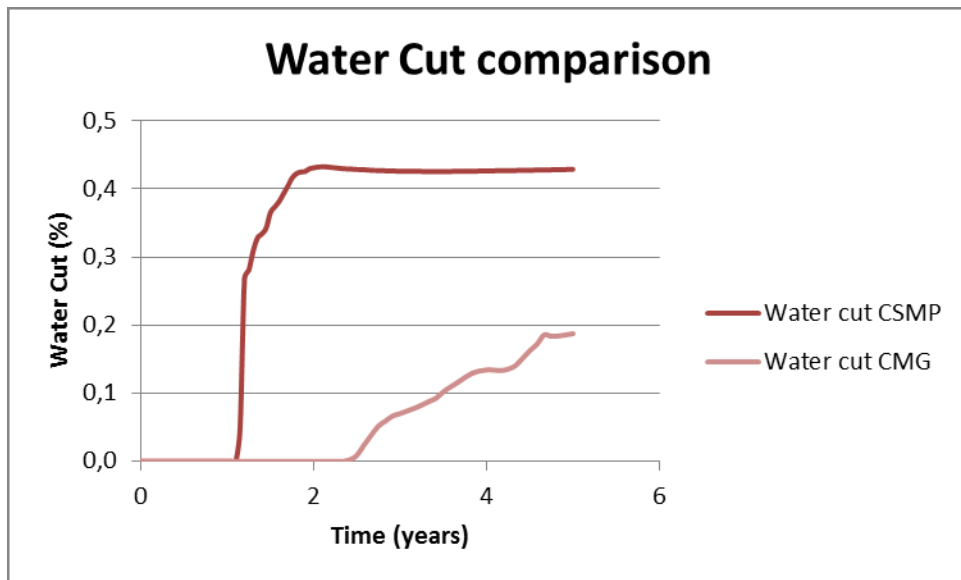r shaped grid blocks and grid resolution is obtained just in the small layers for example in the Bunt sandstein, which is a reservoir layer. However, grid resolution near the faults is not obtained, which makes it impossible to track and observe the events near the faults especially in the zones where small layers are intersecting the faults. This can produce misinterpretation of the flow behavior and furthermore fails in the representation of the instabilities like water coning and viscous fingering.

On the other side, CSMP++ model is constructed in Rhinoceros and meshed in ICEM CFD and uses an unstructured grid, which allows for the possibility of grid refinement near faults and important layers. The CSMP++ model is refined near all of the 19 faults, and near reservoir layer (Bunt-sandstein) in order to capture the small changes which happen there. Thin layers are also more refined.

All of these properties cause the simulators to behave different, and as a product, give different results.

As mentioned in Chapter 6, LGR near wells is very important as well as refinement around the faults and reservoir layers. By using LGR, it is possible to record the flow behavior near wells but this can cause other problems, as previously mentioned, such as numerical stability and very small time-steps. This refinement is also obtained in CSMP++ model, which can be seen in the Figure 33. This is one of the reasons why CSMP++ simulation takes longer than CMG simulation. In order to represent the reservoir in a realistic way, in this case, one should choose in a smart way which properties to sacrifice in order to get the results faster and more accurately. So lately, this question has been of debate, because the question is how to get the results more accurately, but at the same time quickly.

This is why the simulators need to be benchmarked and improved step by step.

Figure 33 and 34 show the comparison of the grid refinement in CSMP and CMG. The obvious difference comes from the point that CSMP uses unstructured grid (triangular mesh), while CMG uses structured grid (rectangular mesh). Grid refinement for CSMP is

done in the meshing tool (ICEM CFD), in CMG this is done directly in the reservoir simulator.
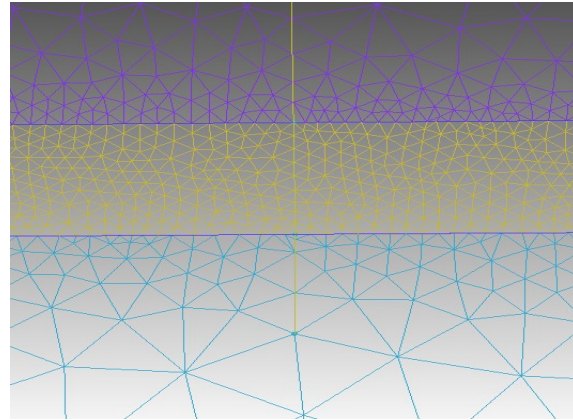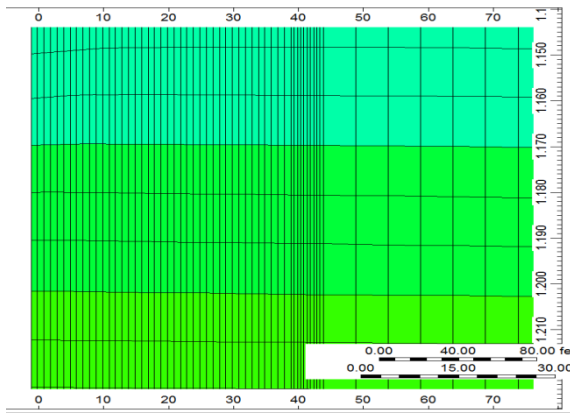

Figure 33: Grid refinement around and at the injector in CMG

Figure 34: Grid refinement around the injector in CSMP

The refinement is very useful to track the changes that happen during the simulation, like instabilities, especially around the wells. The refinement in ICEM CFD has been done around the wells and in the reservoir layer, to be able to capture the changes happening there (since reservoir layer is the most important for the simulation).

However, after the grid refinement in CMG, it was not possible to see any changes in the representation of the instabilities in the simulation.

Different viscosities of the water and oil causes instability in the oil saturation front. The injected water has viscosity of 0.5 cP and viscosity of the oil is 1.7 cP. This behavior is shown in the Figures 35 and 37, water influx is shown in Figures 36 and 38.

The oil saturation front advances faster in the reservoir layer (because of the high permeability and high porosity) and in the layer muchelkalk aquifer. In the layer between these two (muschelkalk aquitard) oil saturation front moves very slow (low permeability and low porosity) (Figure 35 and 37).

Water influx near producer, as shown in Figure 36 and 38, causes early water breakthrough in CSMP. However, the effect of the water influx in CMG is not that strong and it does not cause water breakthrough. The water influx is caused by the presence of the OWC contact at the bottom boundary.
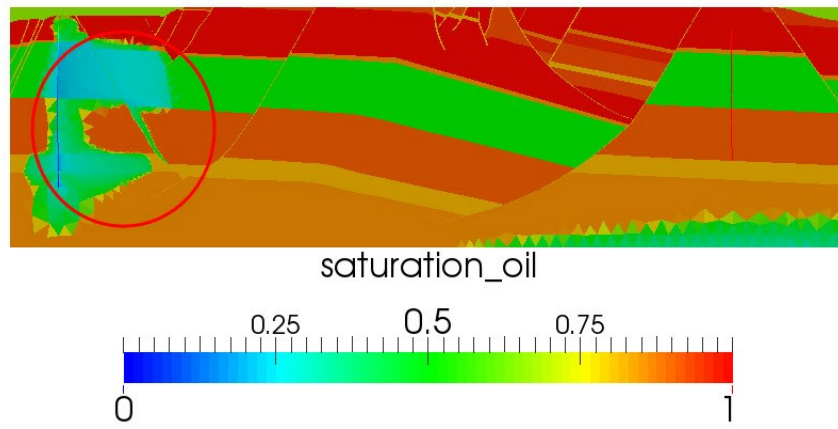
**Figure 35: Oil saturation instability (viscous fingering)
in CSMP simulator**
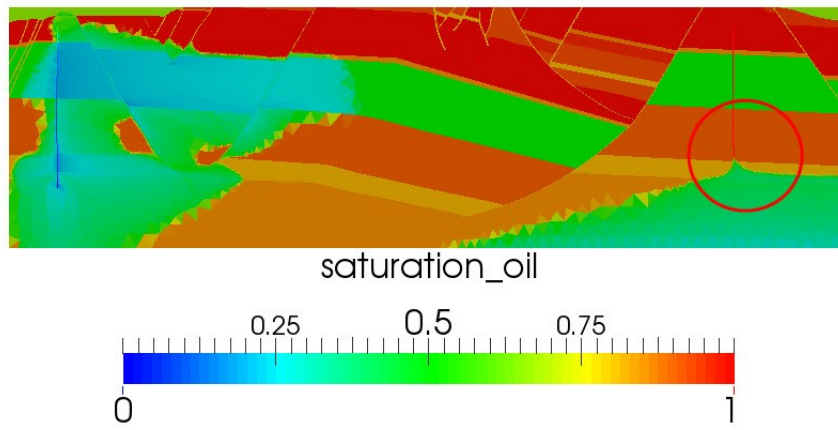
Figure 36: Water influx caused by OWC contact
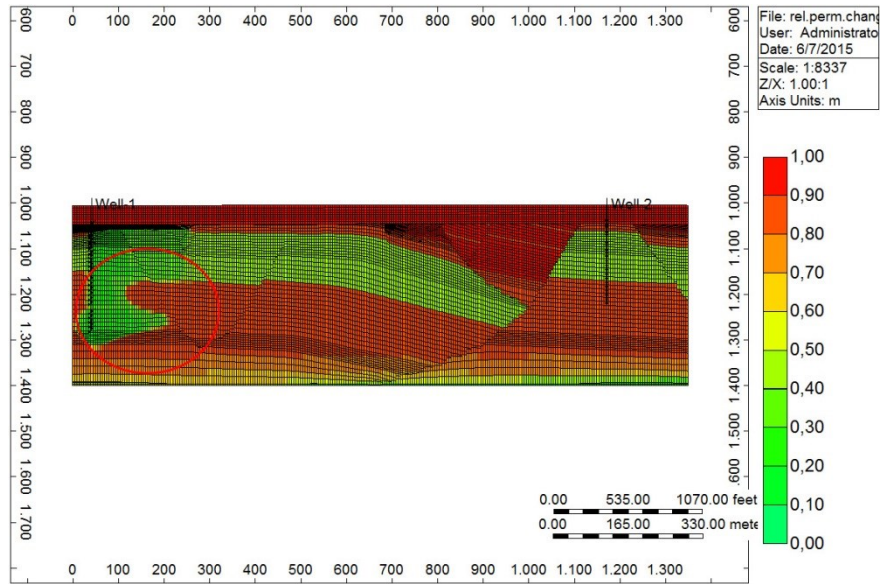
Figure 37: Oil saturation instability (viscous fingering) in CMG simulator
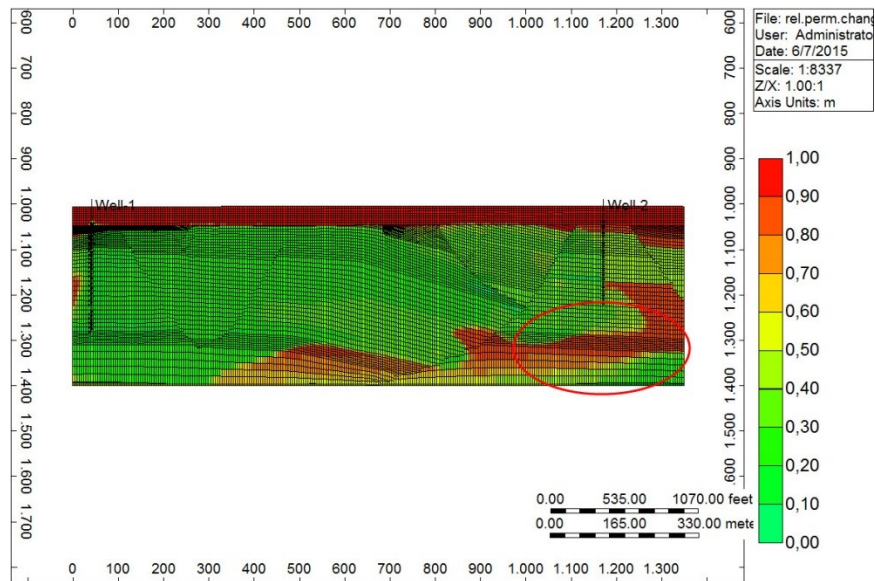
Figure 38: Water influx from the bottom boundary in CMG

Cumulative oil production

Cumulative oil produced is compared for two cases.

1) CASE 1

Figure 39 shows cumulative oil production of CMG and CSMP++, respectively, after 5 years of simulation. It can be seen that cumulative oil produced in CSMP++ is lower than in CMG. The difference is about 4000 m³, which is about 12% difference.
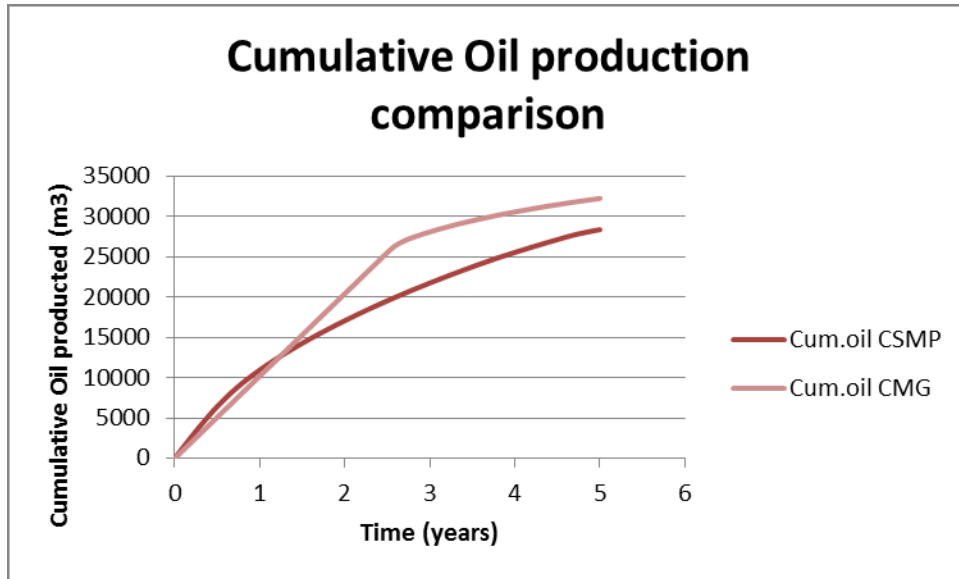
Figure 39: Comparison of the cumulative oil production between CSMP and CMG simulation

2) CASE 2

Figure 40 shows the comparison of the cumulative oil production between the two simulators. The difference is about of 11.6% which is almost the same as in CASE 1.
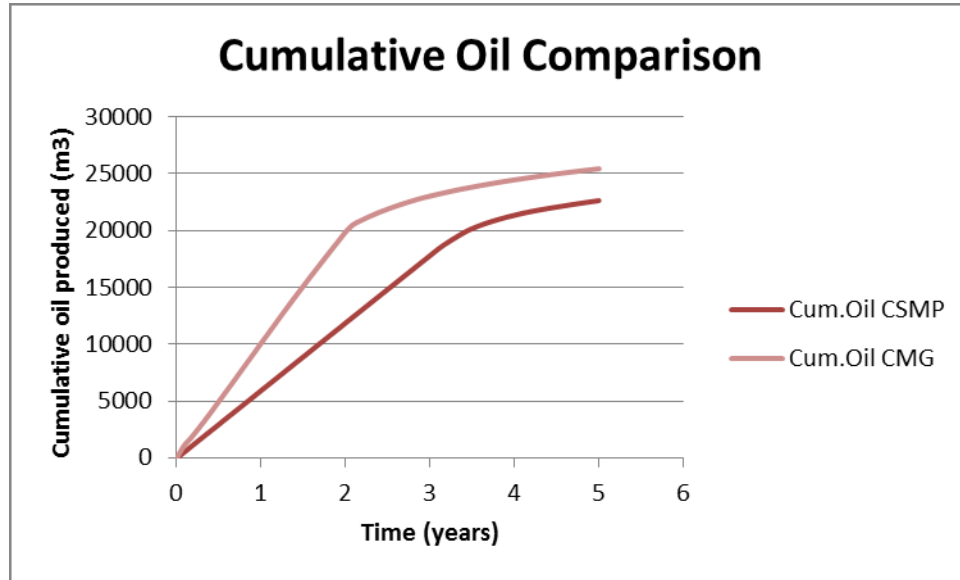
Figure 40: Comparison of the cumulative oil production between CSMP and CMG simulation

Flow velocity distributions

Flow velocity distribution is observed for two cases.

1) CASE 1

Figure 41 and 42 show a comparison of the pressure distribution after 5 years of simulation. The pressure distribution looks quite similar but the pressures values in CMG are double of those in CSMP.

When we look at the oil saturation front, it can be observed that the fronts look pretty similar in both simulators. The difference is greater around lower left corner, in CSMP simulator this area is completely saturated by water. The reason can be the presence of OWC which has great influence in CSMP. It has been concluded that in CMG this property does not affect the saturation front so much. However, there is also one part of the model which is not saturated by water in CSMP, which can be due to the permeability contrasts in this area that pose as an obstacle to the flow. The same problem is observed in CMG near the bottom boundary in the middle and near the producer.

Another important parameter is fluid rate. As previously mentioned, both injection and production rates are the same in both simulators, but the simulators have different ways of prescribing this property. The difference is that the CSMP simulator is prescribing a uniformly distributed rate across the well, while the CMG is adjusting this rate according to the permeabilities (in the area of the high permeabilities, velocities are usually very high and vice versa). This causes pressure in the CMG to be higher than in the CSMP simulation. Additionally, no flow boundaries cause high pressure to accumulate near the boundaries.
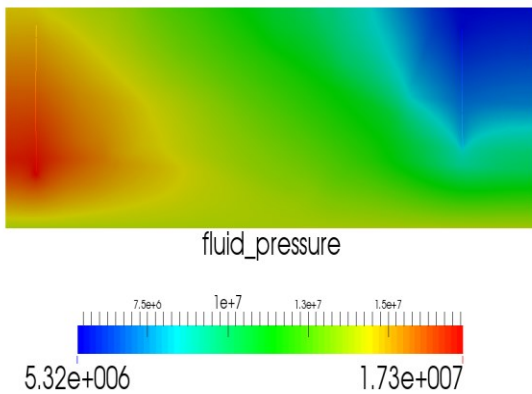
Figure 41: Pressure distribution in CMG in kPa (after 5 years)
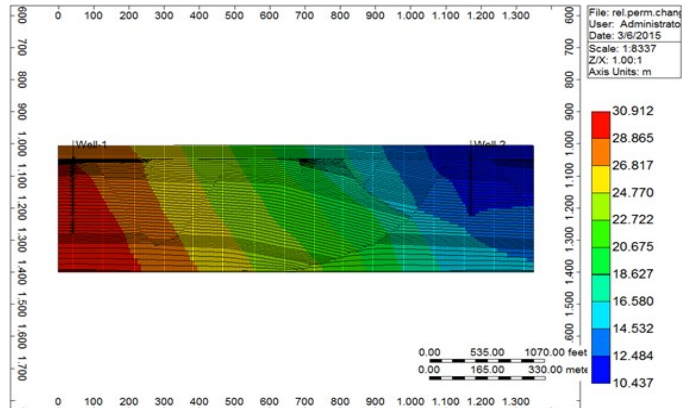
Figure 42: Pressure distribution in CSMP in Pa (after 5 years)

Figures 43 and 44 show an oil saturation front comparison after 5 years of the simulation. The figures show agreement between the results, so the oil saturations fronts look quite similar, except in the middle which is still oil saturated in CSMP. It is possible that the simulator encounters a problem in simulating the surrounding of the intersection of the fault (high permeability) and Muschelkalk aquitard (low permeability layer).

Figure 43: Oil saturation front in CMG after 5 years

Figure 44: Oil saturation front in CSMP after 5 years

Figures 45, 46, 47 and 48 show the comparison of the oil velocities (flow rates) between the simulators. These figures show quite different values of the flow rates, although the injection and production rates are the same. It can be observed that: in CSMP minimum flow velocity is 1E-09 m/s (8.64E-05 m/day) and maximum is 9.31E-05 m/s (8 m/day). The maximum flow velocity is around the producer.

Figure 45: Oil velocity near injector in CSMP (m/s)
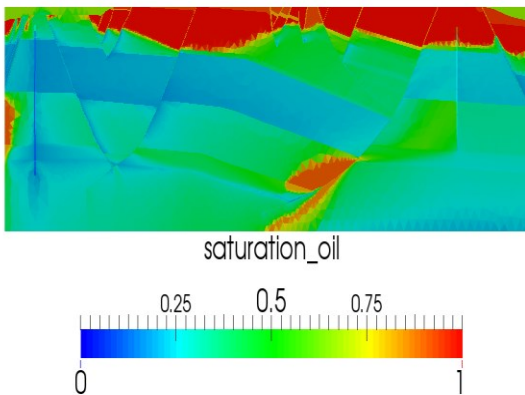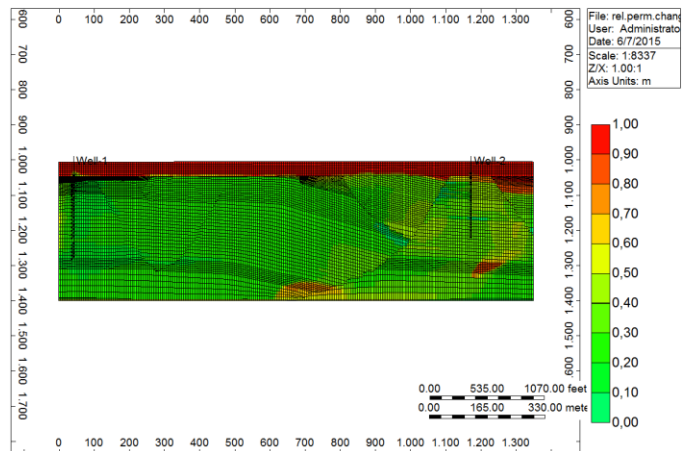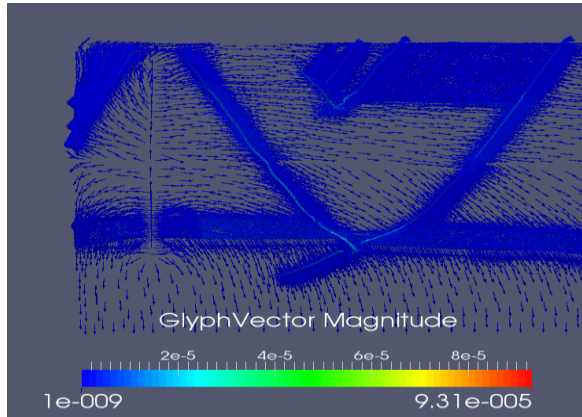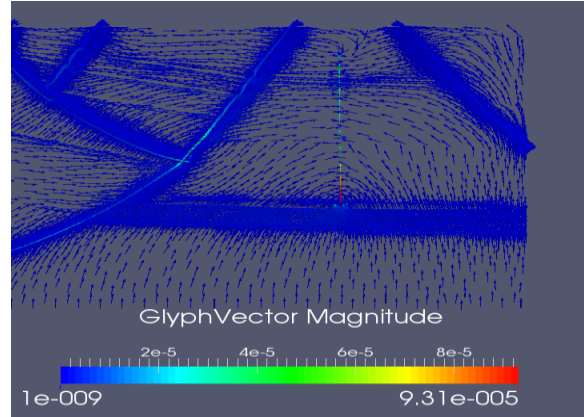

Figure 46: Oil velocity near producer in CSMP (m/s)

In CMG minimum flow velocity is -0.07 m/day (negative value comes from the fact that the figure shows velocity in x direction). The maximum is 0.71 m/day.

The flow velocities distribution does not show the agreement between the two simulators. One of the reasons for this, besides different discretization methods, is transmissibility. From the Figures 40 and 41, it can be seen that flow is strongly dominated by the faults, and the velocities in the fault are pretty high. This behavior can be seen in the CMG simulator.

Transmissibility can be combined into Darcy's law. This is influencing the fluid flow and flow velocities distributions significantly. The following formula shows the Darcy's law,

$$q_o = \frac{k \cdot k_{ro}}{\mu_o} A \frac{p_{oi} - p_o}{\Delta x} \tag{5.1}$$

which can be then re-written into formula combined with transmissibility,

$$q_o = T \left(\frac{k_{ro}}{\mu_o} \right) A (p_{oi} - p_o) \tag{5.2}$$

which shows that k (effective permeability), A (cross sectional area) and x (distance at which q is calculated) is strongly influencing the transmissibility, and by that calculation of the flow velocity. As seen in the comparison of the faults permeabilities, the permeability of

the fault is applied through the transmissibility multiplier, and not the permeability itself, which means that the fault permeability is strongly influenced by the transmissibility.

The transmissibility of the faults is needed because of the presence of stair-step faults, where the grid blocks are not perfectly in line, so with the cross section area, the transmissibility is calculated and applied, what makes the calculation of the flow velocities around the faults possible and allowing the flow to go through the faults.
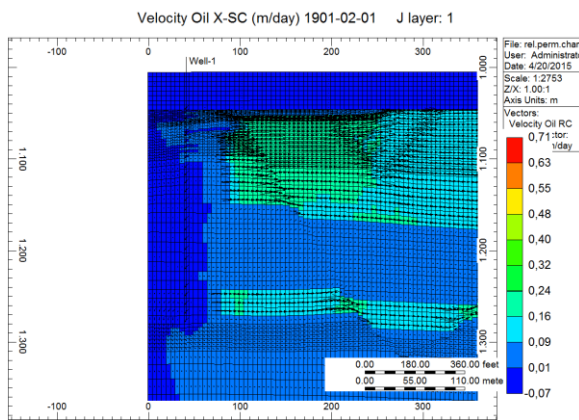
Figure 47: Oil velocity near injector (CMG) (m/day)
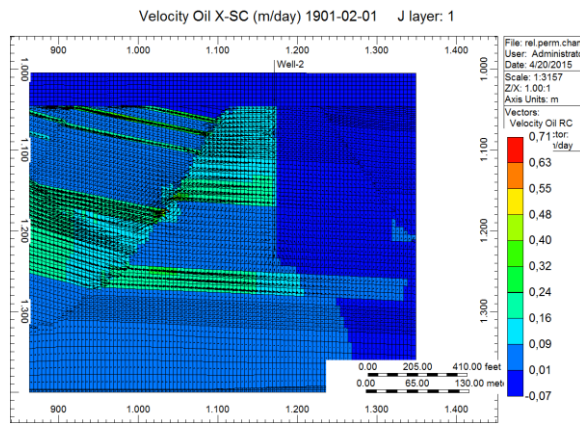
Figure 48: Oil velocity near producer (CMG) (m/day)

2) CASE 2

Figure 49 and 50 show the comparison of pressure distribution between two approaches.

Note that in both simulations is produced with 1000 kPa of bottom-hole pressure and injected with 28.3 m^3/day. To be able to converge in CMG (implicit time-step discretization have difficulties with obtaining the result if the time-step is too large), minimum time-step was reduced to 0.0001 s.
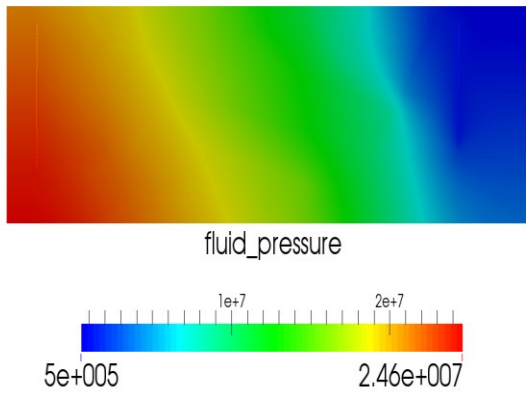
Figure 49: Fluid pressure in CSMP after 5 years (Pa)
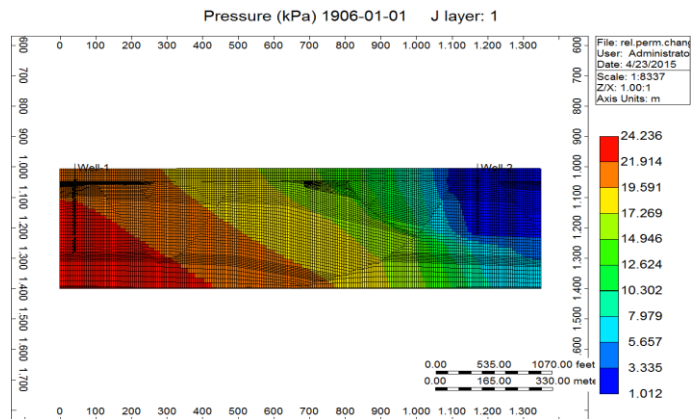
Figure 50: Fluid pressure in CMG after 5 years (kPa)

Fluid pressure distribution shows very good agreement of both simulators. With the minimum of 5 bar and maximum of 246 bar in CSMP, and minimum of 10 bar and maximum of 242 bar in CMG, this comparison shows better results compared to the CASE 1, regarding the fluid pressure distribution.

Figure 51 and 52 shows pretty good agreement for oil saturation front in both simulators.
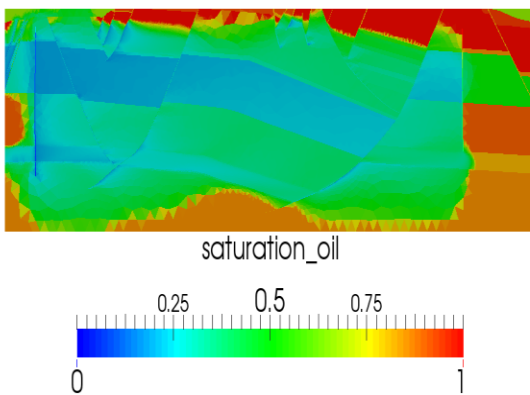
Figure 51: Oil saturation after 5 years in CSMP (Pa)
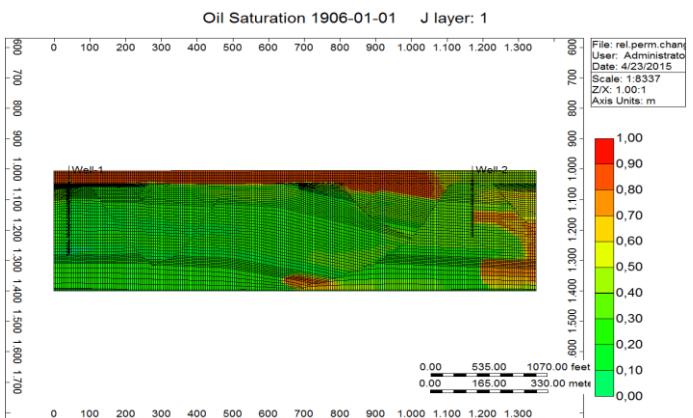
Figure 52: Oil saturation after 5 years in CMG (kPa)

Figures 53, 54, 55 and 56 show oil velocity distribution around the injector and producer.

It can be observed almost the same behavior as in the CASE 1. The maximum velocity is around the producer.

CMG shows the maximum oil velocity of 0.63 m/day, which is much lower than the maximum velocity of the CSMP. The flow is strongly dominated by the faults, which have bigger velocities than the surroundings. This behavior cannot be observed in CMG.
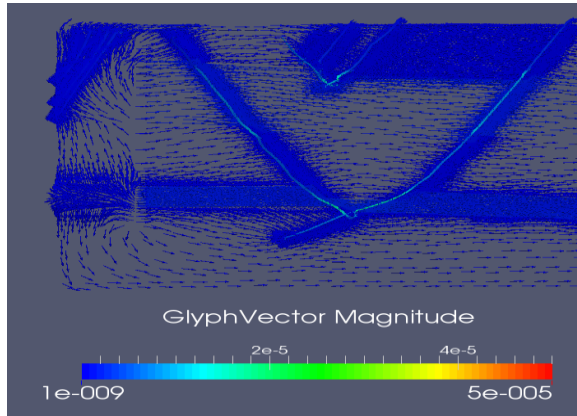
Figure 53: Oil velocity near injector in CSMP (m/s)
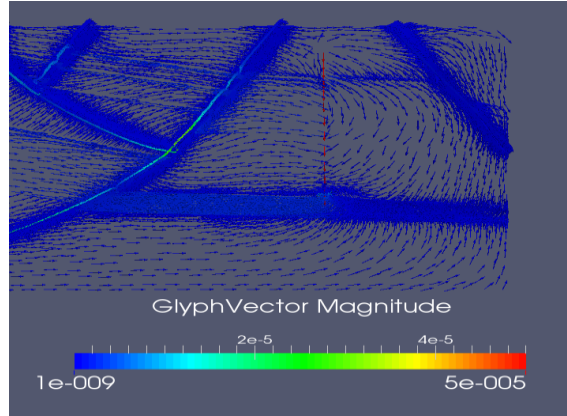
Figure 54: Oil velocity near producer in CSMP (m/s)
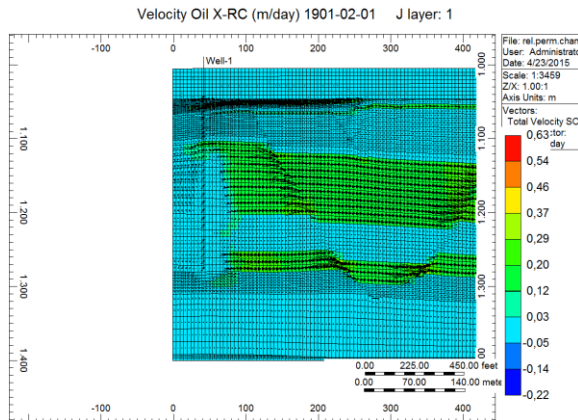
Figure 55: Oil velocity near injector (CMG) (m/day)
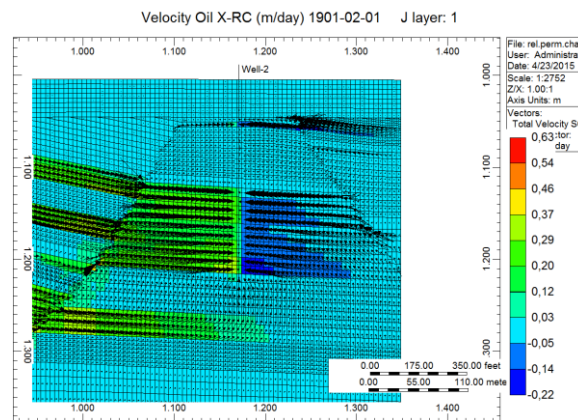
Figure 56: Oil velocity near producer (CMG) (m/day)

Analytic versus discrete well model

Figures 57 and 58 show, the difference between two approaches for discretization and representation of the wells. While the FECFV approach uses discrete well representation, the FD approach supports an analytical well model in which material properties are averaged between adjacent grid cells. This means that the properties cannot vary discontinuously, from element to element. On the other hand, an unstructured grid (discrete well model) is different from a structured grid (analytic well model) in the way that the neighbor information cannot be obtained by simple operations. It is required that the tree-graph (the finite element mesh) has dynamic and multidirectional connectivity. This can be associated with runtime and storage problems, but has also an advantage- the material properties that have constant value in one group have to be stored just once.

A) Discrete well representation


Figure 57: Discrete well representation for CSMP++ simulation

Well is represented by a line (in the middle) and is connected to the small triangular elements. The use of triangular elements with piece-wise constant properties supports discrete material interfaces.

B) Analytic well representation
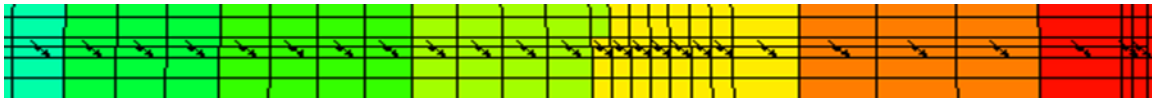
Figure 58: Analytic well model for CMG simulation

The well is represented by a line (in the middle) which is connected to the rectangular grid blocks and is perforated through every grid block. Material properties are averaged between adjacent grid cells.

Types of intersections of structures/layers and high layer-fault aspect ratio

If we compare Figures 7 and 9, one can see that an unstructured grid permits faults' intersections at lower angles than a structured grid, because of the different discretization (division into smaller elements- in unstructured grid- triangles, in structured grid-rectangles-grid blocks). So it can be seen that an unstructured grid permits sharper intersections between adjacent layers and faults, which allows us to represent geology in a more realistic way.

Figure 59 shows the meshed model in ICEM CFD, from which it can be observed that the area near faults is more refined, which allows us to track the velocities profiles and the behavior of the flow near faults and also in very thin layers more accurately.
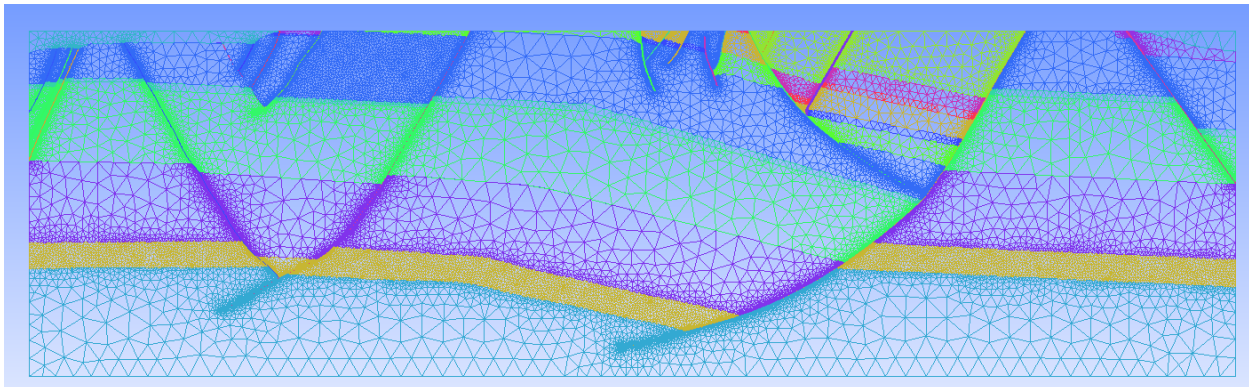
Figure 59: Meshed model in ICEM CFD

Figure 60 shows the intersection of the layers and one of the faults in ICEM CFD. Figure 61 shows the intersection of the same layers with the same fault in CMG. It is obvious that the representation of the structured grid is used in a completely different way to represent it. This way is called a 'stair-step' representation of the faults. In this kind of representation, diagonal components of the surface or a line, are represented by stair-stepping the diagonal with the approximately horizontal tops, bottoms and sides of the model's grid cell. This kind of geometry misrepresents the modeled position of the fault for many operations, which can cause problems in exploration and modeling.
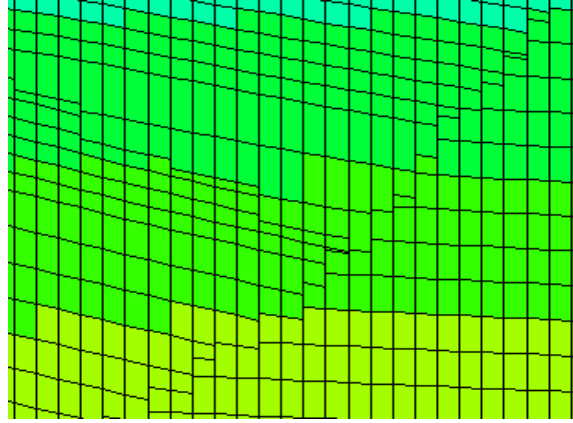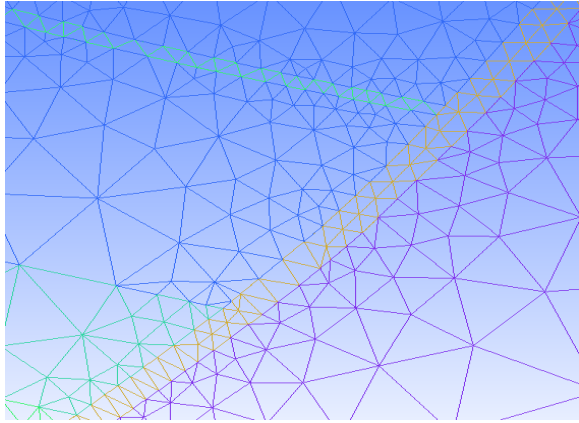
Figure 60: Intersection of the layers and the fault in ICEM CFD

Figure 61: Intersection of the layers and the fault in CMG

The correlation between thickness and width are commonly used for particular geological bodies and this numerical relationship is called *aspect* ratio (Gluyas, 2004). In the complex model, aspect ratios are very high, which can cause the problems as failure to capture instabilities like viscous fingering and water coning. This problem is related to the grid orientation effects as well.

Because the values of the S_{oi} and S_{wi} are taken from the literature, therefore the k_{ro} and k_{rw} as well as viscosities are already calculated with the given values, the mobility ratio in the most of the layers is higher than 1. To be able to compare the grid orientation effects and the influence of the mobility ratio on the failure to capture the instabilities, different mobility ratios should be applied and compared. Unfortunately, there was not enough time to do this comparison, as the time for the thesis planned was 6 months full time work.

58

Permeability contrasts

The reservoir near Chienberg tunel in Switzerland consists of 14 different rock types with low, intermediate and high permeability. The low permeability layer resides at the top and is called Opalinus clay and restricts the flow.

In the areas of change from one layer to another, from high to low permeability or the reverse, there is difficulty for the oil saturation front to advance and there is obvious distortion of the flow. I also observed problems related to the time of the simulation in the CSMP which are caused by big differences in permeability. These differences are around 10E-8 and if increased, the time step decreases, which means that simulation time increases.

Figure 62 shows permeability distribution in the reservoir. The highest permeability is in the reservoir layer bunt-sandstein and muschelkalk aquifer. In Chapter 7 it is explained the velocity distribution, where it can be seen that velocity is highest around the area with higher permeability and the flow focuses on the areas with increased permeability, because in these areas there are no barriers to flow.
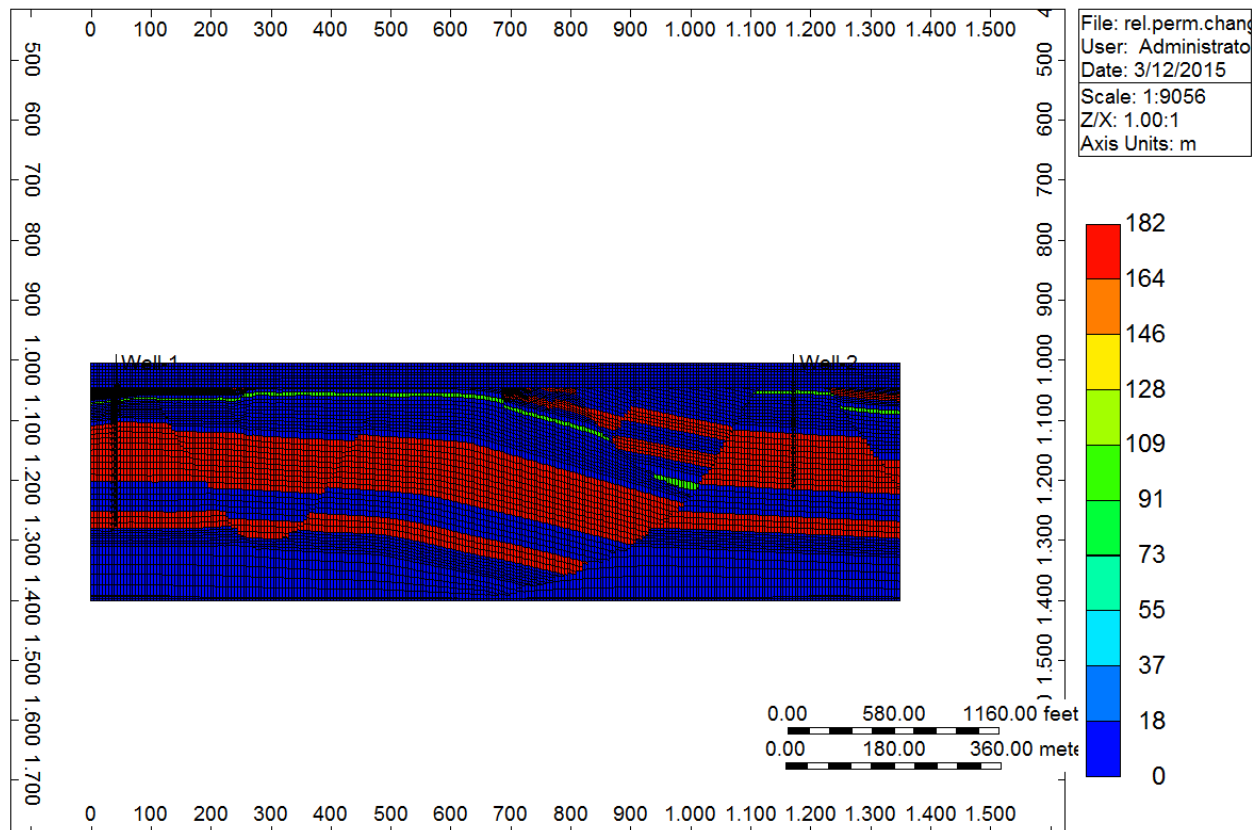
Figure 62: Permeability distribution of the reservoir in CMG in mD

Fault permeability contrasts

Since the flow of th Chienberg model has been highly dominated by the faults, it is very important to observe the behavior of the faults permeability contrasts. This will be presented in this chapter.

CSMP++ Simulator

In this paragraph, the comparison between different permeability of the faults within the two simulators and its impact on the fluid flow distribution and recovery factor is investigated.

Figures 63 and 64 show the oil saturation fronts after 5 years of simulation in CSMP simulator for two different cases: low permeable and impermeable faults. The injector uses water volume source of 1.31e-06 m^3/m^3s and producer fluid volume source of -1.31e-06 m^3/m^3s. It can be observed that regarding the oil saturation fronts, there is a huge difference between these two cases, as expected. In Figure 63, it can be observed that faults are, due to the very low permeability, behaving as obstacles to flow, so flow concentrates on the area before faults, because faults stop the oil saturation front from progressing further. In the case of low permeability faults, the oil saturation front is quite similar to the oil saturation front of the case with the highly permeable faults (Figure 49).
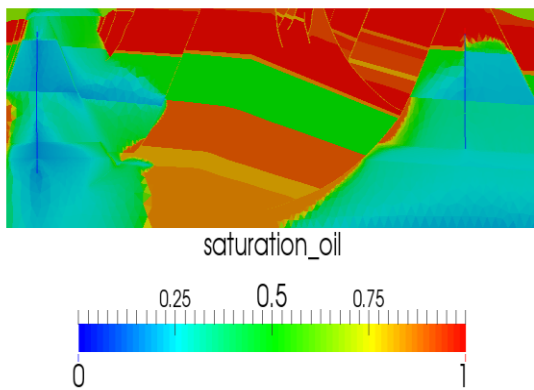
Figure 63: **Oil saturation front after 5 years (imperm. faults)**
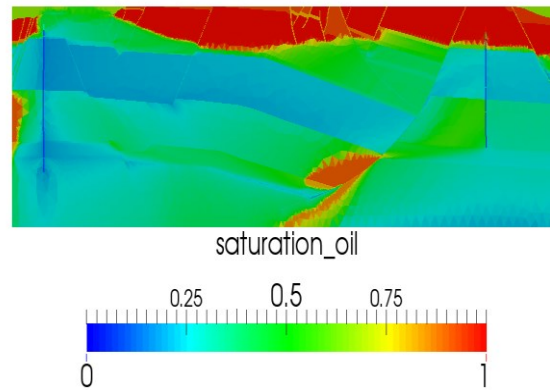
Figure 64: Oil saturation front after 5 years (low perm. faults)

Comparison of highly permeable (1.82 D), low permeable (1.82 mD) and impermeable faults (0.0182 mD)

CSMP simulator

Figure 65 and 66 show a big difference between the reservoir with highly permeable faults and the reservoir with impermeable faults with respect to the cumulative oil produced and recovery factor. The differences between the reservoir with highly permeable faults and the reservoir with low permeable faults are very small.
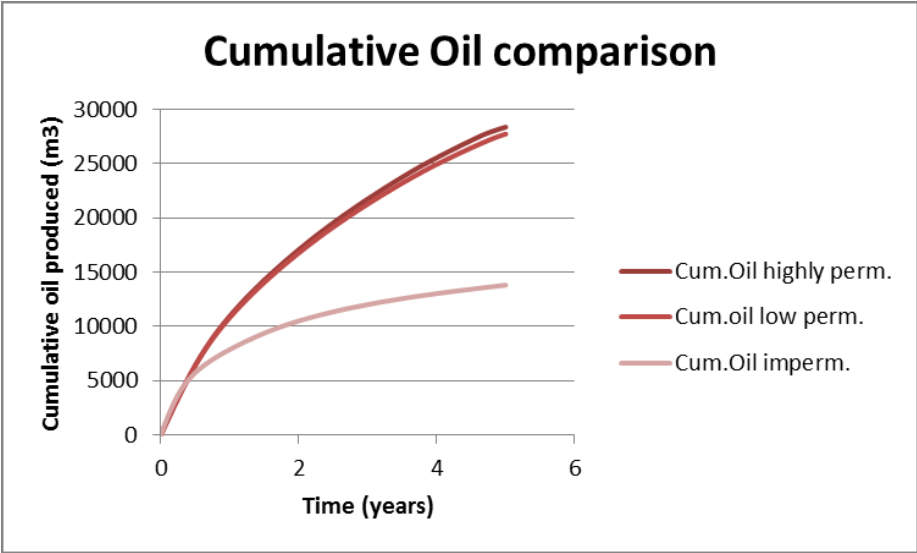
Figure 65: Comparison of the Cumulative Oil produced between the reservoirs with highly permeable faults, low permeable faults and impermeable faults
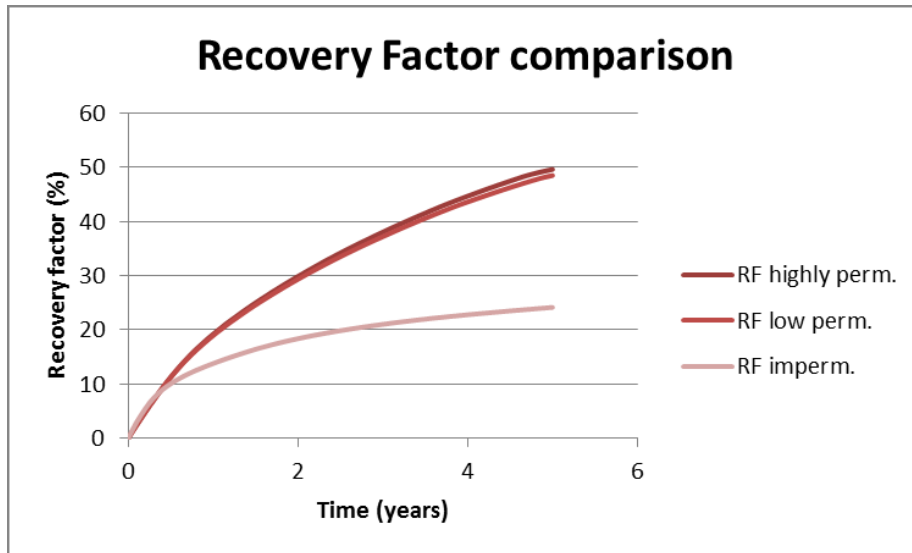
Figure 66: Comparison of the Recovery Factor between the reservoirs with highly permeable, low permeable and impermeable faults

CMG simulator

Figure 67 shows the end of the simulation (after 5 years). The transmissibility multiplier is set to 0. Injection and production rate are 28.3 m³/day. CMG shows a similar behavior as CSMP. The flow is stopped at the first barrier, which is a fault in this case, and moves forward around the fault. The fault is acting as an obstacle to the flow.
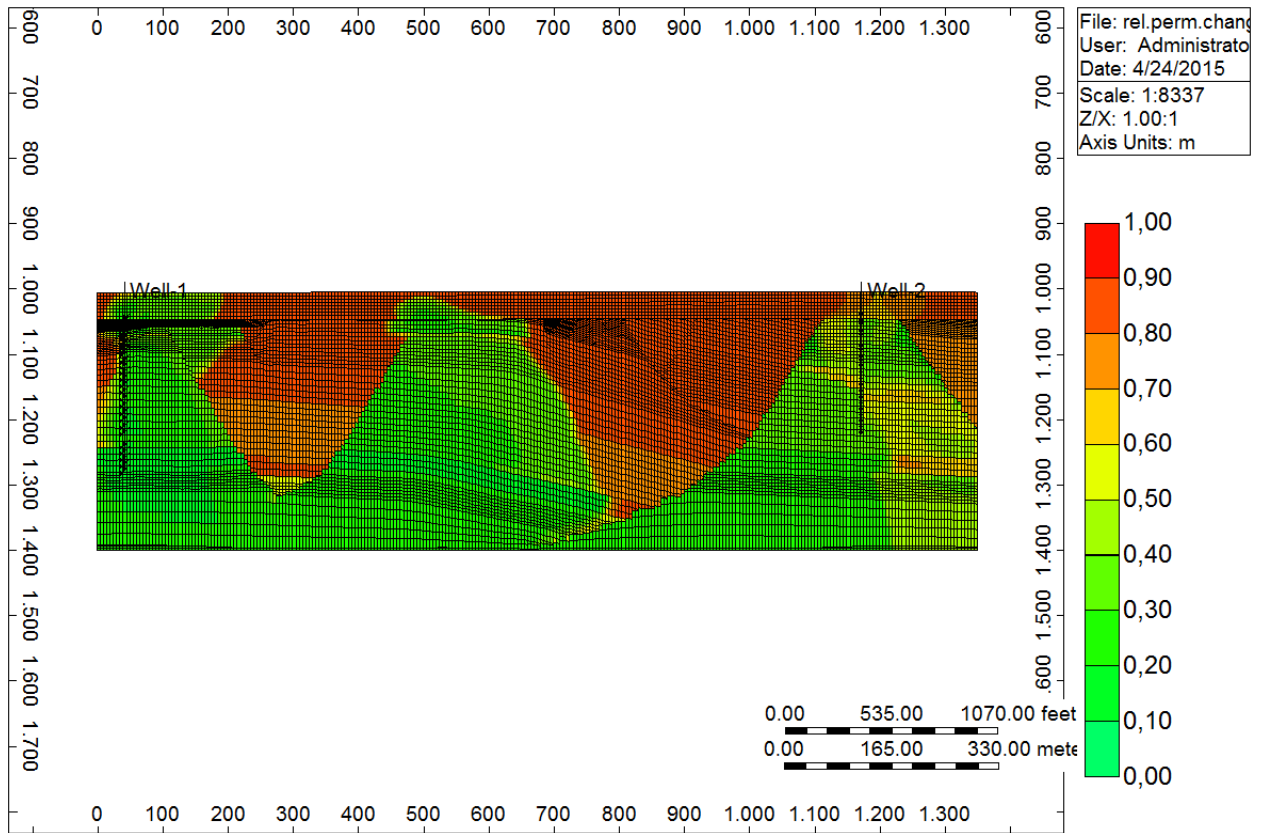
Figure 67: Oil saturation front after 5 years of simulation (transmissibility multiplier set to 0)

The cumulative oil comparison between the models with different transmissibility is shown in Figure 68. As expected, cumulative oil production is significantly decreases after setting transmissibility to 0. This makes faults to be sealed and therefore it is harder to recover oil from the reservoir.
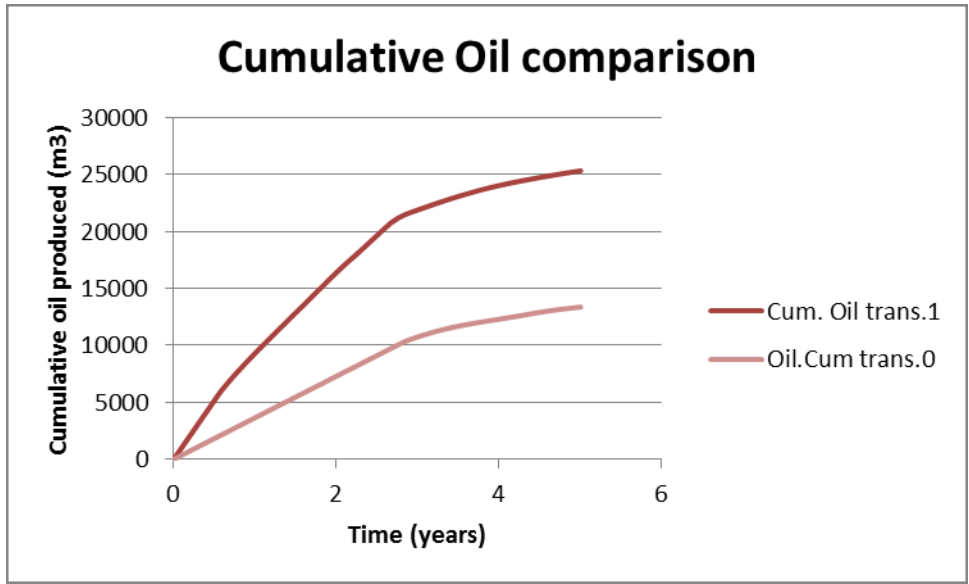
Figure 68: Cumulative oil comparison between the models with transmissibility 0 and 1 in CMG simulator

Figure 69 shows the comparison of recovery factors. The simulator shows the expected behavior and the recovery factor is much lower than in the case of the transmissibility 1. When tried to simulate with the rate of 28.3 m³/day, the simulator showed the convergence error, which could not be overcome by reducing the time step size. In order to simulate without errors, injection and production rates are lowered to the 10 m³/day.
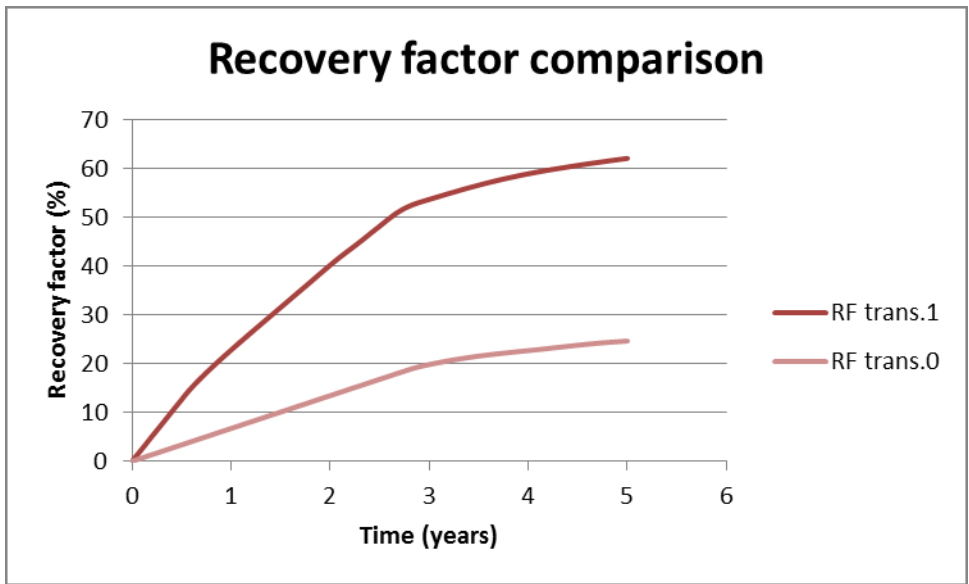
Figure 69: Recovery factor comparison between the models with transmissibility set to 0 and 1 in CMG simulator

6. Conclusions

As already observed in the simulation of the Test model, comparison between the two simulators by using the source terms in CSMP and the rates in CMG did not yield any acceptable result. The problem with source terms in CSMP is that fluid pressure cannot be easily controlled, and because of this, Dirichlet pressure needs to be specified at one of the boundaries, which in this case is the bottom boundary. Immediately, in the first time-step, it can be observed that the pressure distribution does not look the same, and this leads to differences between the results. Defining an aquifer at the bottom boundary in CMG was the best solution to try to overcome these differences, unfortunately without success.

As compared in the Figures 10 and 13, in the Test case, recovery factor and cumulative oil production curves have different shapes, and obviously, different percentages. Oil velocity distribution is very different as well, with a different range of values. These are shown in the Table 9, which shows the results summary for the test model.

Table 7: Summary of the results for test model

	CSMP		CMG		% difference	
Property	CASE 1	CASE 2	CASE 1	CASE 2	CASE 1	CASE 2
Pore volumes (m3)	123200	123200	123200	123200	0	0
OIIP (m3)	100115	100115	101760	101760	1.62	1.62
WIP (m3)	23731	23731	23400	23400	1.4	1.4
RF (%)	20	54.14	36	54.52	16	0.38
Cumulative Oil (m3)	20000	54037	36519	55483	58	2.64
Fluid pressure decline (bar)	83	146	163	226	87	43
Oil velocities (MAX-MIN) (m/day)	6.69	0.02546	0.083	0.106	195	122
Time to breakthrough (year)	0	3.6	0	5	0	1.4

Once more, it is important to mention, that in CMG it is not possible to model incompressible flow. In incompressible flow, B_o tends to be 1, and R_s constant, which is impossible to model in CMG without obtaining errors.

A compromise must be made. B_o is modeled in the way that it is monotonically increasing (like incompressible fluid), but on the other side these increases are very small (tending to model compressible fluid). R_s values are kept nearly constant, with monotonical increase. The changes in modeling B_o and R_s in CMG are making a huge differences on the OIIP and pore volumes predicted, which is further making great differences in the prediction of oil recovery.

The conclusion drawn after the simulation of the test model is that using source terms and rates is not a good reference point for the comparison between these two simulators, because of specific problems with converting the sources to the rates and accounting for the well diameter (this is because the wells in 2D are lines).

In the simulation of the complex model, it is proven that CASE 2 gave better agreement between the results, which is explained in the results.

The reason why the complex model gave better results in the CASE 1 than the test model is of further discussion.

Both simulators need improvement because of the particular problems related to it. For example, due to the convergence error, while simulating with the bottom-hole pressure, the maximum time-step size needed to be reduced. Otherwise, the simulator produced an error. This time-step error is related to the implicit time discretization, which has problems with convergence if the time-step is too large. Table 10 shows the summary of the results for the complex model.

Table 8: Summary of the results for the complex model

Property	CSMP		CMG		% difference	
	CASE 1	CASE 2	CASE 1	CASE 2	CASE 1	CASE 2
Pore volumes (m3)	88892	88892	73323	73323	19.19	19.19
OIIP (m3)	56426	56426	54950	54950	2.65	2.65
WIP (m3)	20185	20185	17365	17365	15	15
RF (%)	50	40	58	49	8	9
Cumulative Oil (m3)	28390	22647	32271	25448	12.79	11.64
Fluid pressure decline (bar)	124	241	205	232	49	3.8
Oil velocities (MAX-MIN) (m/day)	8.03	4.31	0.64	0.41	170	165
Time to breakthrough (year)	0.7	1.2	1.6	2.6	0.9	1.4

The CSMP simulator needs to be improved in terms of computational time, because it is taking longer than CMG simulations. CSMP simulation of the Chienberg model takes approximately 1 day, while CMG finishes it in approximately 3 hours.

Both cases did not show good agreement with the results of the fluid velocities. As previously explained, this has to do with the transmissibility.

In the comparison of the different permeability of the faults, both simulators behaved the same. When the transmissibility multiplier is set to 0, the faults act as sealing agents, and do not allow the flow to go through. When set to 1, the faults are completely permeable and the flow moves across the faults. CSMP shows the same behavior, when low and high permeability is used. Changing the transmissibility multipliers, shows that the transmissibility is a major component in CMG for matching the two results and simulating the models with a lot of faults. The complex model is strongly dominated by the flow in the faults, therefore strongly influenced by the transmissibility.

After the long observation and comparison, it is concluded that both simulators however need to be improved in the future. CMG has its difficulties related to handling complex geometries and the user's understanding but the biggest advantage over CSMP is that it is capable of modeling black oil compressible flow. CSMP is already improved to two-phase,

slightly compressible flow, but it is not used in this thesis due to the technical problems. However, the Reservoir Institute of the University of Leoben is working hard to make further improvements on this simulator.

7. References

Bazr-Afkan, S. (2012). Investigation of Gas-Oil Gravity Drainage in Naturally Fractured Reservoirs using Discrete Fracture and Matrix Numerical Model. Leoben: Dissertation, University of Leoben.

Behrenbruch, P. e. (1985). Probabilistic Hydrocarbon Reserves Estimation: A Novel Monte Carlo Approach. SPE 13892/1.

Berteig, V. e. (1988). Prediction of Hydrocarbon Pore Volume with Uncertainties. SPE 18325.

Brand, C. H. (1991). The Grid Orientation Effect in Reservoir Simulation. SPE 21228.

Butscher, C. e. (2011). Relation between hydrogeological setting and swelling potential of clay-sulfate. Engineering Geology 122 (2011) 204–214.

Chavent, G., Jaffre, J. (1986). Mathematical Models and Finite Elements for Reservoir Simulation. North Holland, Amsterdam.

Chong, E. S. (2004). A Unique Grid-Block System for improved Grid Orientation. SPE 88617.

Delfiner, P. C. (1977). Conditional Simulations: A new Monte Carlo approach to probabilistic evaluation of hydracarbon in place. SPE 6985, 1-5.

Elkaddifi, K. e. (2004). Bottom-Water Reservoirs, Simulation Approach. Canadian International Petroleum Conference, 1-4.

Geiger, S. D. (2006). Multiphase Thermohaline Convection in the Earth's Crust: I. A New Finite Element –Finite Volume Solution Technique CombinedWith a New Equation of State for NaCl–H2O. Transport in Porous Media, Springer 2006, 399-434.

Gluyas, J. S. (2004). Petroleum Geoscience. Blackwell Publishing.

Group, C. M. (2013). User's Guide IMEX: Three-Phase, Black-Oil Reservoir Simulator.

Heinemann, Z. e. (1991). Modeling Reservoir Geometry with Irregular Grids. SPE.

Holloway, C. K. (1975). Reduction of Grid Orientation Effect in Reservoir Simulation. AIME.

Karimi-Fard, M. D. (2012). Accurate Resolution of Near-Well Effects in Upscaled Models Using Flow Based Unstructured Local Grid Refinement. SPE 141675.

Khalid, A. S. (1979). Petroleum Reservoir Simulation. London: Applied Science Publishers LTD.

King, M. e. (2006.). Optimal Coarsening of 3D Reservoir Models for Flow Simulation. SPE 95759.

King, M. J. (2011). On The Tyranny of Corner Point Grids. Long Beach, CA: SIAM Geosciences Conference.

Mateo, J. R. (2002). Simulation of a Volcanic Naturally Fractured Reservoir: A Case History. Canadian International Petroleum Conference, 1-3.

Muggeridge, A. e. (2013). Recovery Rates, Enhanced Oil Recovery and Technological limits. Royal Society publishing.

Murtha, J. (1997). Monte Carlo Simulation: Its Status and Future. SPE,JPT.

Rautenbacher, L. (2013). Characterization and Development of Hypothetical Reservoir in Switzerland with Emphasis on Analysis of Water Injection Rates. Bachelor thesis, Montan university of Leoben.

Rodrigues, L. C. (2007). Incorporating Geomechnics into Petroleum Reservoir Numerical Simulation. SPE 107952.

Steven C. Chapra, R. P. (2010). Numerical Methods for Engineers. McGraw-Hill.

Stone, H.L., Garder, A.O. (1961). Analysis of Gas Cap or Dissolved-Gas Reservoirs. SPE AIME 222, 92-104.

Strausser, J. (1976). Computer Analysis of Reserves using Pore-Volume Method. SPE 6326, 1-4.

Welte, D. W. (2002). From Static to Dynamic Interpretation of Subsurface Data-. AAPG Explorer.